

The reaction $\pi N \rightarrow \omega N$ in a dynamical coupled-channel approach

Yu-Fei Wang,^{1,*} Deborah Rönchen,¹ Ulf-G. Meißner,^{2,1,3} Yu Lu,⁴ Chao-Wei Shen,¹ and Jia-Jun Wu⁴

¹*Institute for Advanced Simulation and Jülich Center for Hadron Physics,
Forschungszentrum Jülich, 52425 Jülich, Germany*

²*Helmholtz-Institut für Strahlen- und Kernphysik (Theorie) and Bethe
Center for Theoretical Physics, Universität Bonn, 53115 Bonn, Germany*

³*Tbilisi State University, 0186 Tbilisi, Georgia*

⁴*School of Physical Sciences, University of Chinese Academy of Sciences, 100049 Beijing, China*

(Dated: October 24, 2022)

A refined investigation on light flavor meson-baryon scatterings is performed using a dynamical coupled-channel approach, the Jülich-Bonn model, that respects unitarity and analyticity constraints. The channel space of πN , $\pi\Delta$, σN , ρN , ηN , $K\Lambda$ and $K\Sigma$ is extended by adding the ωN final state. The spectra of N^* and Δ resonances are extracted in terms of complex poles of the scattering amplitudes, based on the result of a global fit to a worldwide collection of data, in the energy region from the πN threshold to center-of-mass energy $z = 2.3$ GeV. A negative value of the ωN elastic spin-averaged scattering length is extracted, questioning the existence of bound states of the ω meson in the nuclear matter.

I. INTRODUCTION

The scattering of light mesons and baryons, starting from the pion-nucleon channel, has been a topic of interest for many decades and continues to be so. On the one hand, such reactions reveal crucial information to obtain a deeper understanding of the strong interaction, on the other hand, the output from the study of such scattering processes can be used as input for further research, such as nuclear structure or nuclear astrophysics. On the fundamental level, Quantum Chromodynamics (QCD) governs the hadronic interactions. However, due to color confinement, QCD cannot be applied directly when the energy is not high enough. To deal with non-perturbative problems at low energies, chiral perturbation theory [1–11] was developed, based on the spontaneously broken chiral symmetry of light flavor quarks and regarding the light hadrons as basic degrees of freedom, with the pseudoscalar mesons being the quasi Goldstone bosons. By perturbative expansions in the meson masses and the momenta, the near-threshold observables can be well reproduced, see e.g. [12–19], and some low-lying resonances e.g. the $\Delta(1232)$ isobar and the Roper resonance can also be treated, see e.g. [20–29].

Another challenging subject is the intermediate energy region: though experimental observations are abundant, the dynamics becomes more involved as more interaction channels open, and theoretical approaches are further complicated by the appearance of a large amount of resonances. In this region, the effective field theory description breaks down while perturbative QCD is not yet applicable. Extracting the resonances from experimental data is, thus, a fundamental task of great importance, which cannot be trivially accomplished, since most of the states do not exhibit a typical Breit-Wigner

behavior. To attack this problem, efforts were made by partial wave analyses [30, 31] restrained to πN elastic scattering, resulting in most of the resonances known today. However, due to the fact that some states may not couple strongly to πN [32], coupled-channel analyses are also necessary. Straightforwardly, the phenomenological inputs can be unitarized or re-summed [33–38], reproducing unitary amplitudes with complex poles on the unphysical Riemann sheet as the resonances. Furthermore, though complicated, coupled-channel models evolving under dynamical scattering equations [39–55] do not only keep the unitarity but also globally lead to a better analytical behavior with fewer model artefacts in the complex energy plane.

The approach applied in this paper is called the Jülich-Bonn (JüBo) model, which has experienced three decades of development. Its core is a Lippmann-Schwinger-like equation, taking tree-level diagrams and correlated two-pion exchange as the kernel. Based on early studies on meson-meson and K^-N interactions [39–41], the approach was first applied to πN elastic scattering in Refs. [42, 43]. Its early coupled-channel extensions (including $\pi\pi N$ and ηN) can be found in Refs. [44–46]. In Ref. [49] the analytical structures of the amplitudes obtained by this model are systematically studied, enabling the extraction of resonances as poles in a modern way. In Refs. [50, 51], the model has progressed to the zero-strangeness kaon-hyperon channels $K\Lambda$, $K\Sigma$ and higher partial waves up to $J = 9/2$, with the center-of-mass energy up to 2.3 GeV. A major step towards a reliable determination of the light baryon spectrum based on an extensive high-quality data base with the extension of the framework to meson photoproduction was achieved in Refs. [53, 56, 57]. Moreover, in Refs. [54, 55] the approach was adapted to include virtual photons and was applied in the first-ever coupled-channel study of pion and eta electroproduction data. Besides the light meson-baryon scattering and photoproduction processes, the P_c states in the hidden-charm sector were also studied with

* yuf.wang@fz-juelich.de

the JüBo model [58, 59].

To summarize, the hadronic Jülich-Bonn model is one of the theoretically best founded tools for studying the spectrum of the light-flavored baryon resonances. So far, the maximum energy considered in the model is 2.3 GeV but certain channels like ωN have not been considered. To further refine the model and to enrich the resulting physics, here we extend this model by adding the ωN channel. Furthermore, the ω can be considered as the first vector meson regarded as a stable particle in this approach.

Reaching beyond the completion of our model, the ωN channel is of interest for several reasons. It has been found that the spontaneous broken chiral symmetry of QCD shows a tendency of restoration as the density of nucleons gets larger in the nuclear matter, as signaled e.g. by dropping vector meson masses [60–62], although this particular claim is at odds with earlier calculations [63]. Much experimental and theoretical work has been done in this field. On the experimental side, the pertinent signals are usually of electromagnetic nature. For a review, see e.g. [64]. Due to the vector meson dominance [65], the γN interaction is dominated by ρN , ωN and ϕN . The ρ meson is very broad and would not behave like a quasi-particle when it is in-medium, while the direct ϕNN coupling is suppressed due to the nearly pure $s\bar{s}$ component of ϕ . In this respect, ωN can be considered as the most important channel. Additionally, the details of ωN interaction are essential for understanding the equation of state of the neutron stars [66].

According to the low-density theorem [67], the additional in-medium self-energy of the ω is proportional to the elastic scattering amplitude of ωN . Therefore, the elastic ωN amplitude provides crucial information about the in-medium ω . This holds especially for the real part of the spin-averaged ωN scattering length, which indicates whether or not the ω can form bound states in the medium. However, this scattering length cannot be observed directly by experiments. On the theoretical side, even the sign of the spin-averaged ωN scattering length is still an open question. Results based on QCD sum rules [68–70] support an attractive force in the ωN system from the scattering length, contradicting other analyses [34–38, 48, 71–74]. Comprehensive models like the current one, which extract the scattering length constrained by a global fit to all possible data sets, are needed to clarify this issue.

This paper is organized as the follows. In Sect. II we outline the underlying theoretical framework of the model, especially the structure of the scattering equation. All the important information about the fit, like the numerical details and the fit to the data of ωN channel, as well as the two different solutions to estimate the uncertainties, are displayed and discussed in Sect. III. Sect. IV contains the results concerning the hadron spectrum (baryon resonances) and the scattering lengths, with discussions on the resulting physics. Sect. V presents the conclusions of this work and some perspectives for further studies. The expressions for the observables in the ωN channel are shown in Appendix A. The partial wave amplitudes of $\pi N \rightarrow \omega N$ interaction are given in Appendix B. Tables containing the coupling strengths of the resonances to the effective three-body channels ($\pi\Delta$, σN and ρN) are given in Appendix C. Fit results for channels other than ωN can be found on the website [75]. Further details of the theoretical framework are summarized in the supplemental material [76].

II. THEORETICAL FRAMEWORK

In the current study, the πN , $\pi\pi N$, ηN , $K\Lambda$, $K\Sigma$ and ωN channels are considered. The $\pi\pi N$ system is simulated by three effective channels, the $\pi\Delta$, σN and ρN . The threshold of each channel is shown in Fig. 1. Note that the width of the ω meson is much smaller than its mass, and is thus not considered in this work.

The master formula of this model is the following scattering equation:

$$T_{\mu\nu}(p'', p', z) = V_{\mu\nu}(p'', p', z) + \sum_{\kappa} \int_0^{\infty} p^2 dp V_{\mu\kappa}(p'', p, z) G_{\kappa}(p, z) T_{\kappa\nu}(p, p', z), \quad (1)$$

where T denotes the scattering amplitude, V denotes the interaction kernel (the potential), p' and p'' are the three-momenta of the initial and final states in the center-of-mass frame, respectively, z is the center-of-mass energy, which is related to p' and p'' by the on-shell conditions when calculating physical observables. Further, μ, ν and κ are the channel labels denoting the meson-baryon system with specific isospin (I), angular momentum (J , up to 9/2), spin (S) and orbital angular momentum L . $G_{\kappa}(p, z)$ is the propagator of the intermediate channel:

$$G_{\kappa}(z, p) = \begin{cases} (z - E_{\kappa} - \omega_{\kappa} + i0^+)^{-1} & (\text{if } \kappa \text{ is a two-body channel}), \\ [z - E_{\kappa} - \omega_{\kappa} - \Sigma_{\kappa}(z, p) + i0^+]^{-1} & (\text{if } \kappa \text{ is an effective channel}). \end{cases} \quad (2)$$

Further, E_{κ} , ω_{κ} denote the energies of the baryon and the meson in channel κ , respectively, with a relativistic dispersion relation, e.g. $E_{\kappa} = \sqrt{p^2 + M_{\kappa}^2}$. For the quasi

three-body channels, Σ_{κ} is the self-energy function of the unstable particle (Δ, σ, ρ). Note that such kind of propagators are derived from (old-fashioned) time-ordered per-

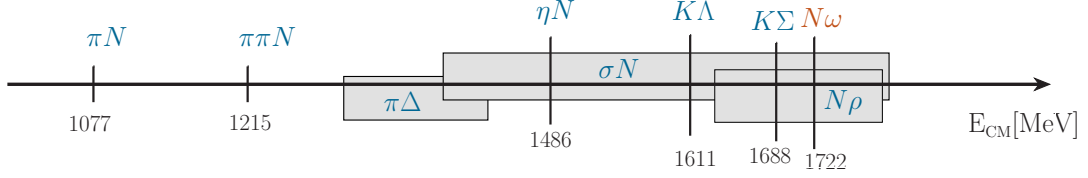


FIG. 1: Thresholds of the scattering channels currently considered in the JüBo model as function of the center-of-mass energy.

turbation theory (TOPT) [77] rather than the modern covariant convention. In combination with a partial-wave projection, the application of TOPT reduces the fully relativistic Bethe-Salpeter equation [78] to the one-dimensional integral of Eq. (1). Accordingly, the potential V is also constructed using TOPT.

In principle the potential V in Eq. (1) can contain any two-particle irreducible term. To simplify the calculation, the following separation is performed:

$$T = T^{NP} + T^P. \quad (3)$$

Specifically, T^{NP} is generated only by potentials from t - and u -channel exchange and contact diagrams, denoted as V^{NP} :

$$T_{\mu\nu}^{NP}(p'', p', z) = V_{\mu\nu}^{NP}(p'', p', z) + \sum_{\kappa} \int_0^{\infty} p^2 dp V_{\mu\kappa}^{NP}(p'', p, z) G_{\kappa}(p, z) T_{\kappa\nu}^{NP}(p, p', z), \quad (4)$$

whereas T^P is constructed via

$$T_{\mu\nu}^P(p'', p', z) = \sum_{i,j} \Gamma_{\mu,i}^a(p'') (D^{-1})_{ij}(z) \Gamma_{\nu,j}^c(p'). \quad (5)$$

Here, i, j are the indices of the s -channel poles, $\Gamma_{\mu,i}^a$ is the dressed vertex function describing the annihilation of the i th resonance to channel μ , and similar for $\Gamma_{\nu,j}^c$ (creation of the resonance from channel ν). Also, D^{-1} is the propagator of the s -channel resonances related to the self-energies Σ_{ij} :

$$\begin{aligned} \Gamma_{\mu,i}^a(p'') &= \gamma_{\mu,i}^a(p'') \\ &+ \sum_{\kappa} \int_0^{\infty} p^2 dp T_{\mu\kappa}^{NP}(p'', p, z) G_{\kappa}(p, z) \gamma_{\kappa,i}^a(p), \\ \Gamma_{\nu,j}^c(p') &= \gamma_{\nu,j}^c(p') \\ &+ \sum_{\kappa} \int_0^{\infty} p^2 dp \gamma_{\kappa,j}^c(p) G_{\kappa}(p, z) T_{\kappa\nu}^{NP}(p, p', z), \\ D_{ij}(z) &= \delta_{ij}(z - m_i^b) - \Sigma_{ij}(z), \\ \Sigma_{ij}(z) &= \sum_{\kappa} \int_0^{\infty} p^2 dp \gamma_{\kappa,i}^c(p) G_{\kappa}(p, z) \Gamma_{\kappa,j}^a(p); \end{aligned} \quad (6)$$

where the γ 's are bare vertices and m_i^b is the bare mass of the i th resonance. Eq. (6) actually corresponds to

the construction of T^P by Schwinger–Dyson-like equations illustrated in Fig. 2. More importantly, T^{NP} can also dynamically generate poles which are not included as genuine states in the s -channel.

The potentials V^{NP} are constructed based on the leading order Lagrangians respecting SU(3) flavor symmetry, C and P conservation, as well as derivative couplings of pseudoscalar mesons from chiral symmetry [79–81]. Except for the correlated two-pion exchange described in detail in Refs. [42, 43], all the other potentials are considered at tree level, causing divergences of the integral in Eq. (4). Hence we add regulators to make the integrals converge, thereby introducing cut-off parameters to be determined by the fit. Such regulators can also be understood as phenomenological form factors, simulating the inner structures of the hadrons. Additionally the integrals in Eq. (6) need similar regulators, but since the bare couplings are already fit parameters, the s -channel cut-offs are fixed.

A more detailed description of the potential can be found in the supplemental material [76]. Note that besides the ωN channel, to make the dynamics of the $K\Sigma$ system complete, in this work we add two more diagrams. These are $K\Lambda \rightarrow K\Sigma$ and $K\Sigma \rightarrow K\Sigma$ reactions with the t -channel a_0 exchange. They are allowed by SU(3) symmetry and other conservation laws, but were not considered in the previous studies using the JüBo model.

Note that the nucleon itself is an s -channel pole, and we always adjust its bare mass and couplings such that the physical values are recovered, for details see Ref. [51]. In addition to the s -, t -, and u -channel diagrams, just as in Ref. [53], we also add phenomenological contact terms to simulate the effects from physics not explicitly contained in the s -, t -, and u -channel diagrams.

The observables can be evaluated using $T_{\mu\nu}$. The normalized, dimensionless partial-wave amplitudes τ are directly related to the observables:

$$\tau_{\mu\nu} = -\pi \sqrt{\rho_{\mu} \rho_{\nu}} T_{\mu\nu}, \quad (7)$$

where ρ is a kinematical phase factor,

$$\rho_{\kappa} = \frac{p_{\kappa}}{z} E_{\kappa} \omega_{\kappa}, \quad (8)$$

and p_{κ} is the corresponding three-momentum. The elements of the unitary scattering S -matrix are also written in terms of τ :

$$S_{\mu\nu} = \delta_{\mu\nu} + 2i\tau_{\mu\nu}. \quad (9)$$

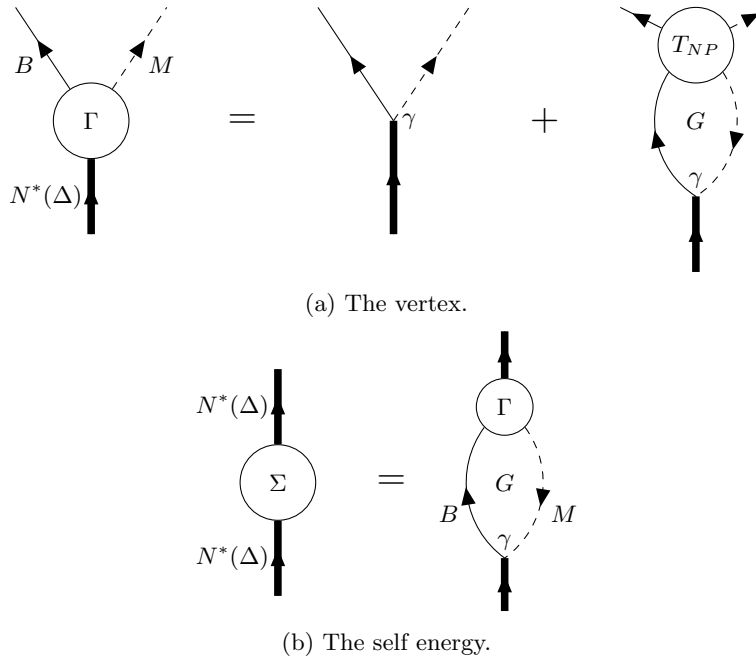


FIG. 2: Schematic plot of Eq. (6).

III. FITS

A. Database and numerical details

For the newly included ωN channel, we fit to the data from the two reactions $\pi^+ n \rightarrow \omega p$ and $\pi^- p \rightarrow \omega n$ simultaneously, in addition to all other channels of the approach. The database for ωN is summarized in Tab. I. The datasets of the channels lower than ωN remain the same as in Ref. [51], see Refs. [30, 84, 87–128]. Note that for the πN elastic scattering we fit to the energy-dependent GWU/SAID solution [30], while the other data points are direct experimental observables. There are approximately 9000 data points in total in our fit. Moreover, the numbers of fit parameters are summarized in Tab. II.

The fits are performed on the JURECA supercomputer at Forschungszentrum Jülich [129], where one node contains 128 processors. Parallel programming is realized by the Message Passing Interface (MPI) in Fortran. Every processor takes a value of energy z , covering the range from the πN threshold to 2.3 GeV. At each energy, the scattering equation Eq. (4) can be solved numerically applying the Haftel-Tabakin scheme [130] by discretizing the integral via Gaussian quadrature and inverting the $(1 - VG)$ matrix algebraically. The χ^2 , measuring the deviation of the theoretical curve to the data points, is minimized by the MINUIT package [131].

As the ωN data base is quantitatively and qualitatively very limited, we apply weighting factors in the χ^2 minimization to force the fit to describe details of the data that would otherwise be ignored. In addition, the

inclusion of the covariance matrices for the $\pi N \rightarrow \pi N$ input from the GWU/SAID solution [132] is postponed to the future. We also note that some data sets exhibit questionable uncertainties (e.g. the ηN differential cross section from Brown et. al. [118]), c.f. the discussion in Ref. [51], so that we refrain from giving χ^2 values here.

Further discussions on the systematic uncertainties of our fit results stemming from the applied model are required. By definition, for a model a systematic error is difficult to determine. We have, however, tried to obtain a rough estimate of the model-dependence by introducing two different fit scenarios and comparing their results:

- Fit A: a solution with dynamically generated poles similar to those in Ref. [51].
- Fit B: starts from an intermediate stage of fit A, with an extra narrow (dynamical) pole in the P_{11} ($J^P = \frac{1}{2}^+$) wave, with a description of the data of equal quality.

An in-depth uncertainty analysis using, e.g., the least absolute shrinkage and selection operator (LASSO) [133] or Bayesian evidence to determine the significance of resonance states, is planned for the future.

B. Description of the data

As for the description of the data, fit B is mainly distinguished from fit A by the πN amplitude of the P_{11} ($J^P = \frac{1}{2}^+$) partial wave, see Fig. 3. In both results there is a (weak) kink when the energy is around 1700 MeV. This is due to the inclusion of the $N^*(1710)$ resonance,

Ref.	Observable	Data points	Reaction
Table. V of Ref. [82]	XS	13	$\pi^+ n \rightarrow \omega p$
Fig. 20 of Ref. [82] (Ref. [83] etc.)	XS	10	$\pi^+ n \rightarrow \omega p$ and $\pi^- p \rightarrow \omega n$
Fig. 14 of Ref. [84]	FWD	10	$\pi^- p \rightarrow \omega n$
Fig. 6 of Ref. [85]	FWD/BWD	34	$\pi^- p \rightarrow \omega n$
Fig. 8 of Ref. [85]	XS	23	$\pi^- p \rightarrow \omega n$
Tab. 1 of Ref. [86]	XS	8	$\pi^- p \rightarrow \omega n$
Fig. 3 of Ref. [86]	DXS	80	$\pi^- p \rightarrow \omega n$
Total	-	178	-

TABLE I: The database of $\pi N \rightarrow \omega N$. “XS” and “DXS” refer to total and differential cross sections, respectively. “FWD(BWD)” refers to the differential cross section for the nucleon forward (backward) direction.

	T^{NP}	T^P	Total
Newly included	15	23	38
Old	64	202	266
Total	79	225	304

TABLE II: The number of fit parameters in this work. See Eqs. (4) and (5) for the separation of T^{NP} and T^P (including the phenomenological contact terms). “Newly included” means the parameters newly introduced by the ωN channel as well as by the two extra a_0 exchange potentials in the $K\Sigma$ channel.

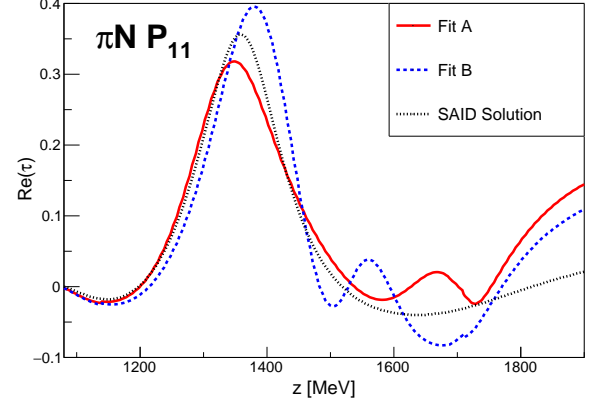
which is absent in Ref. [30]. Furthermore, fit B gives another structure when the energy is around 1500 MeV, which, as an effect from a nearby pole, will be discussed later. Despite such a discrepancy, the global fit qualities are good in both cases.

In the following we only focus on the ωN channel, since the observables of the other channels are the same as in Ref. [51], and the new fit results are shown on the web-site [75]. The expressions of the differential cross section and total cross section are summarized in Appendix A.

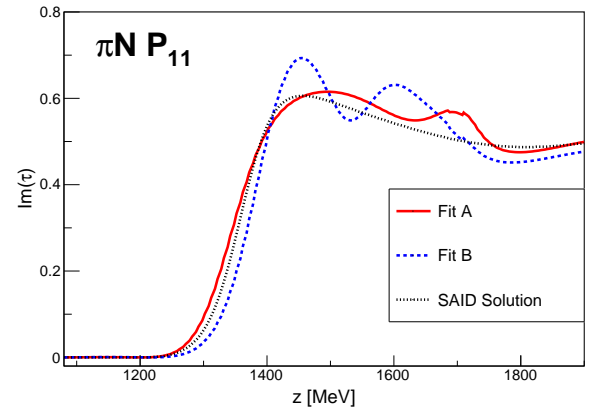
Both fits A and B give a quite good description of the ωN data. The description of the total cross section is shown in Fig. 4. The difference between the two results becomes visible when $z > 1800$ MeV, where the amount of data points decreases. As for the differential cross sections, the results for the nucleon backward and forward directions are displayed in Fig. 5. The curves from fits A and B are quite close to each other, especially when the energy is near the ωN threshold. The angular distributions of the differential cross sections are also fitted well, see Fig. 6.

In this work we just fit to the original experimental data summarized in Tab. I. In addition, there are 30 more points for energies $z = 1800, 1900$ and 2000 MeV, which were actually extracted from the histograms of Ref. [82] by Ref. [35]. As a comparison, we also plot the differential cross sections at those energies in Fig. 7 from our model. It shows that our predictions at these energies are not far away from the data.

At last, based on those two fit results, the partial wave



(a) The real part.



(b) The imaginary part.

FIG. 3: The comparison of fits A and B for the P_{11} πN elastic τ amplitude. The SAID solution is from Ref. [30] (energy-dependent solution).

amplitudes of $\pi N \rightarrow \omega N$ reaction are plotted in Appendix B.

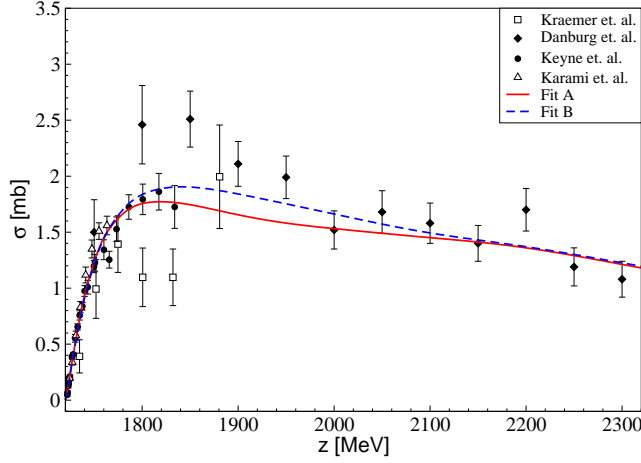


FIG. 4: The total cross section for $\pi N \rightarrow \omega N$ reaction. The data are from Kraemer et al. [83], Danburg et al. [82], Keyne et al. [85] and Karami et al. [86].

IV. RESULTS

A. N^* and Δ spectrum

1. Pole parameters

In this model the resonances are extracted by searching for complex poles of the amplitude τ on the unphysical (i.e. second) Riemann sheet, as described in detail in Ref. [49]. For one resonance pole¹,

$$z_0 = M - \frac{\Gamma}{2}i, \quad (10)$$

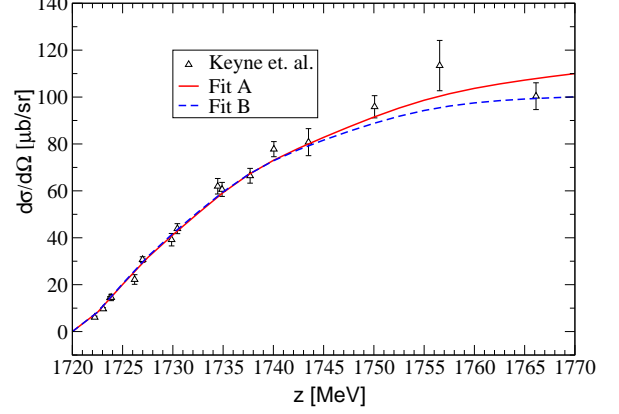
where M is the pole mass and Γ the pole width. The leading order Laurent expansion is parametrized as

$$\tilde{\tau}_{\mu\nu} \sim \frac{R_\mu R_\nu}{z_0 - z} + \dots; \quad (11)$$

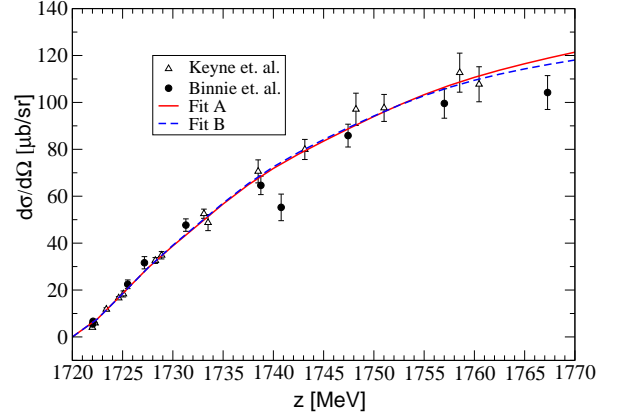
where $\tilde{\tau}$ represents the τ amplitude of the reaction channels $\nu \rightarrow \mu$ on the unphysical sheet, and R_μ is the residue belonging to channel μ . In this paper we use the convention of Partial Data Group (PDG) [134] to measure the coupling strength by the so-called normalized residue:

$$NR_\mu \equiv \frac{2R_{\pi N}}{\Gamma} \times R_\mu. \quad (12)$$

¹ Resonance poles always appear as pairs: when z_0 is a pole then z_0^* must be another. Here we only discuss the one with the negative imaginary part.



(a) Backward differential cross section.



(b) Forward differential cross section.

FIG. 5: The backward and forward differential cross sections of $\pi N \rightarrow \omega N$. The data are from Binnie et al. [84] and Keyne et al. [85].

One can define the nominal partial width in terms of R_μ :

$$\Gamma_\mu \equiv |\sqrt{2}R_\mu|^2. \quad (13)$$

The branching ratios can further be defined via

$$BR_\mu = \frac{\Gamma_\mu}{\Gamma}, \quad (14)$$

and the absolute value of the normalized residue is the transition branching ratio:

$$BR_{\pi N \rightarrow \mu} = |NR_\mu| = \frac{\sqrt{\Gamma_\mu \Gamma_{\pi N}}}{\Gamma}. \quad (15)$$

Note that only when the resonance is an ideal Breit-Wigner state, then the definitions above would meet the common understandings of their names, e.g. the

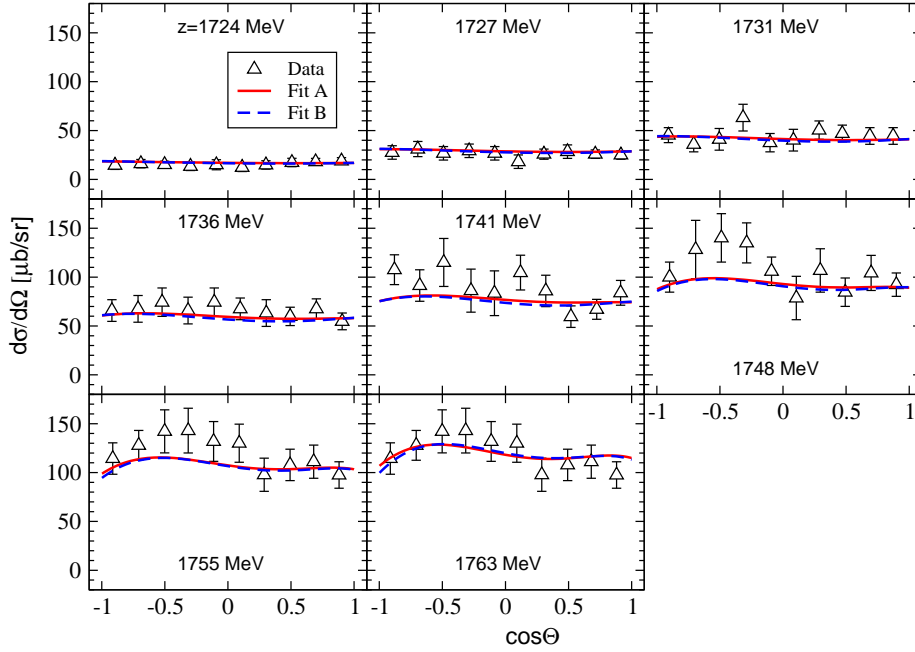


FIG. 6: Differential cross section of $\pi N \rightarrow \omega N$ at different energies. The data are from Ref. [86].

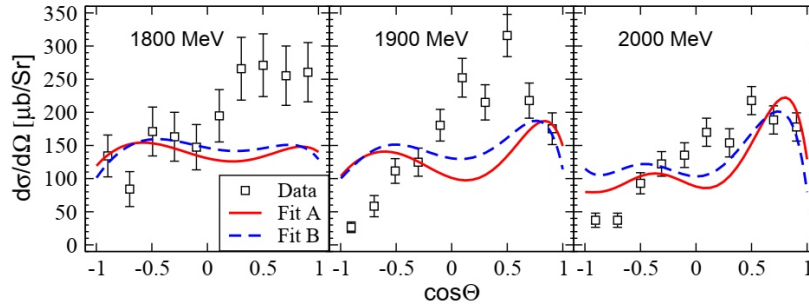


FIG. 7: The $\pi N \rightarrow \omega N$ differential cross sections for the CM energy 1800 to 2000 MeV. The data points were extracted from the histograms in Ref. [82] by Ref. [35], and are not included in the fit. See text for further explanations.

“branching ratios” are understood as the possibilities for the resonance decaying to the final states, which sum up to 100%. Nevertheless most of the N^* and Δ resonances are usually distorted by complicated coupled-channel dynamics, resulting in strong interferences among one another, one has to take those quantities with a grain of salt.

2. Pole positions

First, we list the pole positions of both N^* and Δ resonances within our reach ($\text{Im}(z_0) \leq 450$ MeV) in Tabs. III and IV, respectively. Their locations are also plotted in Fig. 8. We try to assign the names of most poles according to PDG [134]². Some of the pole positions show a

² It must be noted that some of the results published in the PDG tables, especially when it comes to the star rating of the corresponding states, are debatable.

large model-dependence and deviate much from PDG.

As for the N^* states, some well-established states are rather stable in different fits or even different studies (see e.g. Ref. [51]). These are the $N(1535) \frac{1}{2}^-$, $N(1650) \frac{1}{2}^-$, $N(1720) \frac{3}{2}^+$, $N(1520) \frac{3}{2}^-$, $N(1675) \frac{5}{2}^-$ and $N(1680) \frac{5}{2}^+$. It is always hard to determine the high-spin states, but some $J \geq 7/2$ states are stable in this study. In this model the lineshape of the $P_{11} \pi N$ amplitude is dominated by the T^{NP} term, with $N(1710) \frac{1}{2}^+$ being the only genuine s -channel state. This feature has already been found earlier, see e.g. Ref. [45]. It is understandable that the $\frac{1}{2}^+$ poles in fit A derivate from those in fit B, since the two solutions are distinguished by crucial T^{NP} parameters. In the P_{13} partial wave, the $N(1900) 3/2^+$ moved far into the complex plain and is much broader than in JüBo studies including photoproduction reactions [57, 135]. This supports the observation in Refs. [57, 135] and many other studies by different analysis groups that this state is especially important in kaon photoproduction, which is not included in the present work, and hard to determine from purely hadronic reactions. Moreover, the $N(1700) \frac{3}{2}^-$ pole in this work is lower and broader than the estimation in PDG [134]. Last, we emphasize that the $N(1895) \frac{1}{2}^-$, from the coupled-channel analyses of photonproduction in Ref. [136], is of 4-star significance in PDG [134], but until now it *has never been needed in the JüBo model* to obtain a good description of the data.

As already mentioned, the different lineshape of fit B in the P_{11} partial wave, see Fig. 3, stems from an extra narrow resonance at $z_0 = 1585 - 35i$ MeV, with strong couplings to all the channels. However, in fit A this pole moves to $1490 - 245i$ MeV. Indications for similar broad resonance are observed in a recent update of JüBo approach including $K\Sigma$ photoproduction data [135].

Coming to the Δ states, even though ωN is a pure isospin one-half channel, also the $I = 3/2$ parameters are re-fitted as demanded by a coupled-channel framework. Note that some of the T^{NP} parameters do not only change the isospin $I = 1/2$ partial waves and the amount of the data points for the isospin three-half channels is relatively fewer (only $K^+\Sigma^+$ is purely $I = 3/2$). Moreover, the inclusion of the ωN channel has non-negligible effects on the $K^+\Sigma^-$ and $K^0\Sigma^0$ final states as the corresponding threshold energies are close, leading to a rearrangement of the contributions from isospin one-half and three-half. The states of lower partial waves, e.g. the $\Delta(1620) \frac{1}{2}^-$ and $\Delta(1232) \frac{3}{2}^+$, are more stable. However, the $\Delta(1910) \frac{1}{2}^+$, which is of four-star significance in the PDG [134], is very broad in this work, just like Refs. [53, 57]. It seems that the description of the lineshape in the P_{31} wave does not need such a significant resonance signal, see Fig. 9. The two states $\Delta(1920) \frac{3}{2}^+$ and $\Delta(1940) \frac{3}{2}^-$ in our model are significantly broader than the estimation in PDG [134]. Further, the other states tend to be narrower.

3. ωN coupling strengths

In this section we decompose the normalized residue as $NR = |NR|e^{i\theta}$, with θ in units of degrees. Roughly speaking, the modulus $|NR|$ measures how significantly the resonance contributes to the amplitude, while the phase θ controls the interference behavior among different resonances (and the background). The normalized residues of the N^* states for the ωN channel are shown in Tab. V.

In the current fit results, ωN couples mainly to lower-lying states, and the moduli of the normalized residues of the $N(1535) \frac{1}{2}^-$, $N(1710) \frac{1}{2}^+$ and $N(1680) \frac{5}{2}^+$ can be larger than 0.5. Especially the value for the $N(1535) \frac{1}{2}^-$ in channel (1) is more than one. The large couplings to the $N(1535) \frac{1}{2}^-$ and the $N(1710) \frac{1}{2}^+$ may stem from the extremely large bare couplings. At present, we can not determine how model-dependent this result is, and only know that a limited attempt (the fit C) has failed: if we force those couplings to be small, then the fit would always end up in some unphysical local minima with very narrow dynamically generated resonances, and the description of the data is not satisfactory. Maybe further inclusion of the abundant photoproduction data can resolve this issue.

Note that most of the previous studies also support the importance of the lower states in the ωN interaction. For instance, using a quark model, Ref. [137] claims that the $N(1720) \frac{3}{2}^+$ and $N(1680) \frac{5}{2}^+$ have the biggest contributions to ωN photonproduction³, while Ref. [34] gets relatively larger couplings of ωN to $N(1535) \frac{1}{2}^-$, $N(1650) \frac{1}{2}^-$ and $N(1520) \frac{3}{2}^-$. The coupled-channel analyses of Refs. [36–38, 71] indicate the important roles of the $N(1710) \frac{1}{2}^+$, $N(1675) \frac{5}{2}^-$ and $N(1680) \frac{5}{2}^+$. Extremely huge bare couplings can hardly be avoided in phenomenological coupled-channel models, e.g. in Ref. [71], the large bare couplings of ωN to $N(1675) \frac{5}{2}^-$ and $N(1680) \frac{5}{2}^+$ are quite similar to the couplings to $N(1535) \frac{1}{2}^-$ and $N(1710) \frac{1}{2}^+$ here. Note that we do not associate any physical meaning to the bare couplings.

We also list the nominal branching ratios, defined by Eq. (14), of the states above the threshold to the ωN channel, see Tab. VI. Though all those resonances do not couple strongly to ωN , the most significant state is $N(2250) \frac{9}{2}^-$, the branching ratio of which is bigger than 10%. Ref. [37] shows that when photoproduction is included, the $N(1900) \frac{3}{2}^+$ would play an important role among the higher resonances, which is different from the hadronic case here. Ref. [38] has found the branching

³ Unfortunately it is hard to directly compare our result to Ref. [137]. First, the models are completely different, as we regard hadrons as the basic degrees of freedom, and second our coupling strengths are actually labelled by normalized residues.

Resonances	Fit A	Fit B	Estimation of PDG [134]
$N(1535) \frac{1}{2}^-$	$1500 - 46i$	$1499 - 46i$	$1510 - 65i$ (****)
$N(1650) \frac{1}{2}^-$	$1658 - 64i$	$1664 - 68i$	$1655 - 68i$ (****)
$N(1440) \frac{1}{2}^+$ (NP)	$1318 - 126i$	$1411 - 121i$	$1370 - 88i$ (****)
$N(1710) \frac{1}{2}^+$	$1704 - 78i$	$1603 - 279i$	$1700 - 60i$ (****)
$N(1880) \frac{1}{2}^+$ (NP)	$1715 - 233i$	$1755 - 220i$	$1860 - 115i$ (***)
$N(1720) \frac{3}{2}^+$	$1680 - 91i$	$1679 - 95i$	$1675 - 125i$ (****)
$N(1900) \frac{3}{2}^+$	$1717 - 354i$	$1750 - 320i$	$1920 - 75i$ (****)
$N(1520) \frac{3}{2}^-$	$1498 - 53i$	$1499 - 52i$	$1510 - 55i$ (****)
$N(1700) \frac{3}{2}^-$ (NP)	$1439 - 284i$	$1398 - 193i$	$1700 - 100i$ (***)
$N(1875) \frac{3}{2}^-$ (NP)	$1905 - 331i$	$1891 - 261i$	$1900 - 80i$ (***)
$N(1675) \frac{3}{2}^-$	$1658 - 63i$	$1660 - 56i$	$1660 - 68i$ (****)
$N(1680) \frac{3}{2}^+$	$1679 - 46i$	$1674 - 47i$	$1675 - 60i$ (****)
$N(1990) \frac{3}{2}^+$	$1900 - 207i$	$1901 - 204i$	omitted (**)
$N(2190) \frac{3}{2}^-$	$1950 - 180i$	$1960 - 188i$	$2100 - 200i$ (****)
$N(2250) \frac{3}{2}^-$	$2169 - 136i$	$2201 - 145i$	$2200 - 210i$ (****)
2nd pole $\frac{9}{2}^-$ (NP)	$1939 - 213i$	$1978 - 197i$	—
$N(2220) \frac{9}{2}^+$	$2121 - 182i$	$2125 - 182i$	$2170 - 200i$ (****)

TABLE III: Pole positions of the N^* states (in units of MeVs). The first column also exhibits the J^P quantum numbers. “NP” means the pole is possibly dynamically generated from the T^{NP} part. The significance of the states according to the PDG [134] is also shown in the last column.

Resonances	Fit A	Fit B	Estimation of PDG [134]
$\Delta(1620) \frac{1}{2}^-$	$1602 - 44i$	$1602 - 43i$	$1600 - 60i$ (****)
$\Delta(1750) \frac{1}{2}^+$ (NP)	$1882 - 157i$	—	omitted (*)
$\Delta(1910) \frac{1}{2}^+$	$1765 - 339i$	$1813 - 319i$	$1860 - 150i$ (****)
$\Delta(1232) \frac{3}{2}^+$	$1216 - 45i$	$1213 - 44i$	$1210 - 50i$ (****)
$\Delta(1600) \frac{3}{2}^+$ (NP)	$1572 - 81i$	$1577 - 85i$	$1510 - 135i$ (****)
$\Delta(1920) \frac{3}{2}^+$	$1888 - 432i$	$1888 - 427i$	$1900 - 150i$ (***)
$\Delta(1700) \frac{3}{2}^-$	$1825 - 199i$	$1825 - 211i$	$1665 - 125i$ (****)
$\Delta(1940) \frac{3}{2}^-$ (NP)	$2111 - 396i$	$2116 - 412i$	$1950 - 175i$ (**)
3rd pole $\frac{3}{2}^-$ (NP)	—	$1358 - 372i$	—
$\Delta(1930) \frac{5}{2}^-$	$1720 - 293i$	$1711 - 223i$	$1880 - 140i$ (***)
$\Delta(1905) \frac{5}{2}^+$	$1703 - 64i$	$1703 - 63i$	$1800 - 150i$ (****)
$\Delta(1950) \frac{7}{2}^+$	$1884 - 77i$	$1885 - 79i$	$1880 - 120i$ (****)
$\Delta(2200) \frac{7}{2}^-$	$2185 - 84i$	$2208 - 82i$	$2100 - 170i$ (***)
2nd pole $\frac{7}{2}^-$ (NP)	—	$2037 - 324i$	—
$\Delta(2400) \frac{9}{2}^-$	$1942 - 255i$	$1941 - 257i$	omitted (**)

TABLE IV: Pole positions of the Δ states (in units of MeVs). The first column also exhibits the J^P quantum numbers. “NP” means the pole is possibly dynamically generated from the T^{NP} part. The significance of the states according to the PDG [134] is also shown in the last column.

ratio of $N(1875) \frac{3}{2}^-$ to ωN is large, however, this state is not originally included in our model and the position of the dynamically generated one is not stable.

4. Coupling strengths to the lower channels

For completeness, we also show the normalized residues of each resonance for the channels with stable particles lower than ωN . First, the results for the N^* states are given in Tab. VII. The pole positions of the $N(1440) \frac{1}{2}^+$ and the $N(1710) \frac{1}{2}^+$ in fits A and B are not so close to each other, so are their residues. Except for the $N(1535) \frac{1}{2}^-$, $N(1650) \frac{1}{2}^-$ and $N(1710) \frac{1}{2}^+$, all the other

⁴ It is called $D_{13}(1950)$ in Ref. [38].

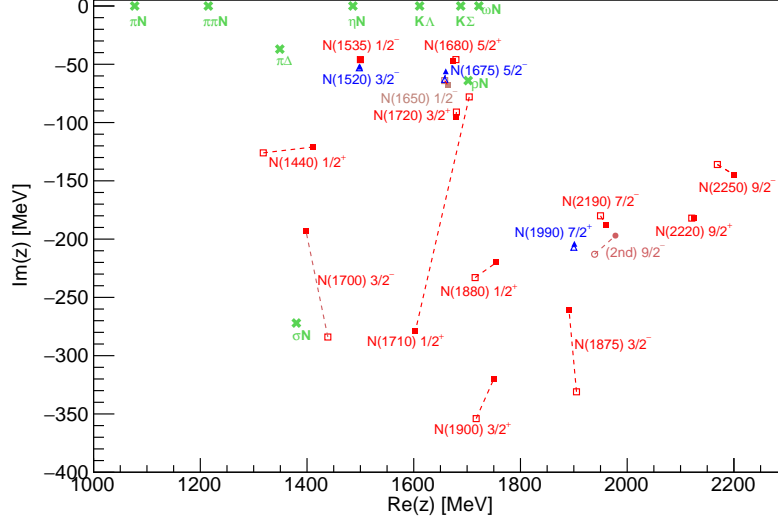
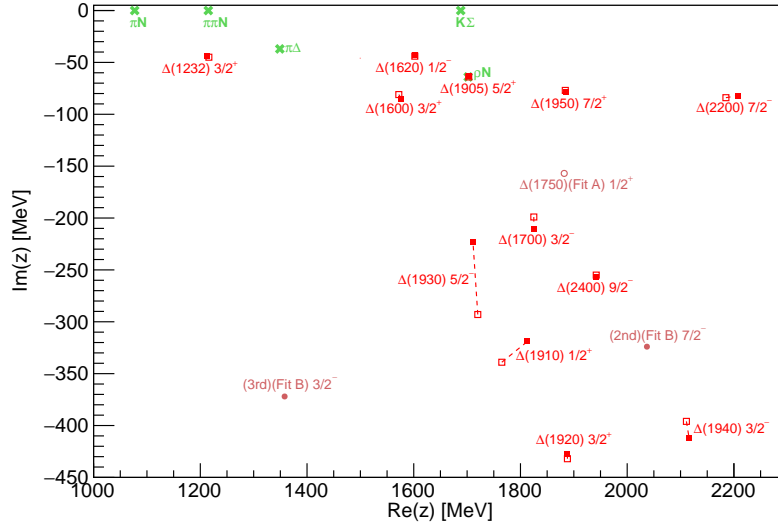
(a) N^* states.(b) Δ states.

FIG. 8: Pole positions from the two fit solutions. Thresholds are labelled by green crosses, and the results of fit A (B) are denoted by empty (filled) symbols.

states do not couple strongly to the KY channels.

The residues of the Δ states are summarized in Tab. VIII. Apart from those states that only show up in fit A or B, the residues of the $\Delta(1910) \frac{1}{2}^+$ and $\Delta(1600) \frac{3}{2}^+$ are less stable. As already discussed, the former tends to be irrelevant to the lineshape in this model, and the latter is affected much by certain T^{NP} parameters.

The branching ratios to the lower physical channels are also given for the N^* states in Tab. IX and for the Δ states in Tab. X. We should emphasize again that the

branching ratios here actually come from the residues, and in principle cannot be directly related to the imaginary part of the pole (the total width). It can happen that these branching ratios do not sum up to 100%, since most of the N^* and Δ resonances are not typical Breit-Wigner states.

Last, currently for the lack of constraints from $\pi\pi N$ and ρN data in this model, the residues for the effective three-body channels are less instructive. Thus, they are displayed in Appendix C.

Resonances	Channel (1)	Channel (2)	Channel (3)
$N(1535) \frac{1}{2}^-$	(1.13, -156°) (1.13, -163°)	0	(0.14, 26°) (0.13, 18°)
$N(1650) \frac{1}{2}^-$	(0.19, 156°) (0.14, 148°)	0	(0.02, -9°) (0.02, -10°)
$N(1440) \frac{1}{2}^+$	(0.18, -37°) (0.21, 23°)	(0.34, 1°) (0.42, 64°)	0
$N(1710) \frac{1}{2}^+$	(0.10, 158°) (0.27, -86°)	(0.56, -172°) (0.73, -59°)	0
$N(1880) \frac{1}{2}^+$	(0.01, -24°) (0.00, 152°)	(0.03, 31°) (0.02, 157°)	0
$N(1720) \frac{3}{2}^+$	(0.01, 150°) (0.01, 155°)	(0.05, -178°) (0.06, -178°)	(0.00, 69°) (0.00, 56°)
$N(1900) \frac{3}{2}^+$	(0.00, 33°) (0.01, -19°)	(0.02, 138°) (0.01, 91°)	(0.00, 6°) (0.00, -75°)
$N(1520) \frac{3}{2}^-$	(0.09, 139°) (0.14, 141°)	(0.04, 102°) (0.07, 115°)	(0.16, -108°) (0.22, -99°)
$N(1700) \frac{3}{2}^-$	(0.02, -35°) (0.03, 20°)	(0.01, -123°) (0.01, 5°)	(0.02, -4°) (0.01, 87°)
$N(1875) \frac{3}{2}^-$	(0.00, -110°) (0.00, -82°)	(0.00, -172°) (0.00, -114°)	(0.00, -157°) (0.00, -105°)
$N(1675) \frac{5}{2}^-$	(0.01, 108°) (0.01, 117°)	(0.25, 82°) (0.30, 89°)	(0.00, -51°) (0.00, -48°)
$N(1680) \frac{5}{2}^+$	(0.00, -8°) (0.00, -32°)	(0.04, 31°) (0.04, 26°)	(0.95, 165°) (0.98, 162°)
$N(1990) \frac{7}{2}^+$	(0.00, -46°) (0.00, -42°)	(0.04, -60°) (0.04, -62°)	(0.00, -105°) (0.00, -107°)
$N(2190) \frac{7}{2}^-$	(0.00, -155°) (0.00, -149°)	(0.01, 146°) (0.01, 154°)	(0.07, 177°) (0.03, 177°)
$N(2250) \frac{9}{2}^-$	(0.01, -31°) (0.01, -47°)	(0.12, -28°) (0.16, -38°)	(0.00, -42°) (0.01, -52°)
2nd pole $\frac{9}{2}^-$	(0.00, 92°) (0.00, 83°)	(0.06, 85°) (0.05, 78°)	(0.00, 44°) (0.00, 44°)
$N(2220) \frac{9}{2}^+$	(0.00, 50°) (0.00, 58°)	(0.01, 10°) (0.01, 14°)	(0.03, 21°) (0.03, 24°)

TABLE V: The normalized residues of the N^* states for the ωN channel. The values are written in the form (NR, θ) , with the phase θ in units of degrees. In each cell, the value of the first (second) row is from fit A (B). The three sub-channels are: (1) $|J - L| = \frac{1}{2}, S = \frac{1}{2}$; (2) $|J - L| = \frac{1}{2}, S = \frac{3}{2}$; (3) $|J - L| = \frac{3}{2}, S = \frac{3}{2}$.

Resonances	Channel (1)	Channel (2)	Channel (3)
$N(1900) \frac{3}{2}^+$	(0.09%)	(0.06%)	(0.00%)
$N(1875) \frac{3}{2}^-$	0.02(0.03)%	0.00(0.01)%	0.02(0.01)%
$N(1990) \frac{7}{2}^+$	0.01(0.01)%	3.20(3.16)%	0.00(0.00)%
$N(2190) \frac{7}{2}^-$	0.00(0.00)%	0.09(0.02)%	3.33(0.79)%
$N(2250) \frac{9}{2}^-$	0.02(0.03)%	12.00(14.23)%	0.03(0.04)%
2nd pole $\frac{9}{2}^-$	0.02(0.01)%	6.65(5.82)%	0.01(0.01)%
$N(2220) \frac{9}{2}^+$	0.00(0.00)%	0.04(0.05)%	0.80(0.87)%

TABLE VI: The branching ratios of the high-lying N^* states to the ωN channel (in percent). The values outside (inside) the brackets are from fit A (B). The $N(1900) \frac{3}{2}^+$ pole in fit A is lower than the ωN threshold. The three sub-channels are: (1) $|J - L| = \frac{1}{2}, S = \frac{1}{2}$; (2) $|J - L| = \frac{1}{2}, S = \frac{3}{2}$; (3) $|J - L| = \frac{3}{2}, S = \frac{3}{2}$.

B. Scattering lengths

The scattering lengths are defined as:

$$a_\kappa \equiv \lim_{p_\kappa \rightarrow 0} p_\kappa^{-1} \tan \tilde{\delta}_\kappa^{(L=0)}, \quad (16)$$

where κ is the channel label and $\tilde{\delta}_\kappa^{(L=0)}$ is the generalized S -wave phase shift from the diagonal element of the S -matrix,

$$S_{\kappa\kappa} \equiv e^{2i\tilde{\delta}_\kappa}. \quad (17)$$

Resonances	πN	ηN	$K\Lambda$	$K\Sigma$
$N(1535) \frac{1}{2}^-$	(0.44, -29°) (0.40, -37°)	(0.48, 126°) (0.48, 120°)	(0.65, 21°) (0.66, 10°)	(0.21, 158°) (0.18, -171°)
$N(1650) \frac{1}{2}^-$	(0.46, -58°) (0.45, -59°)	(0.17, 33°) (0.16, 19°)	(0.21, -68°) (0.21, -74°)	(0.43, -56°) (0.38, -60°)
$N(1440) \frac{1}{2}^+$	(0.40, -104°) (0.57, -74°)	(0.03, -62°) (0.05, 26°)	(0.03, 102°) (0.03, 178°)	(0.04, -47°) (0.03, 176°)
$N(1710) \frac{1}{2}^+$	(0.31, -1°) (0.84, 158°)	(0.51, 161°) (0.54, -129°)	(0.41, -23°) (0.31, 104°)	(0.11, 79°) (0.26, -6°)
$N(1880) \frac{1}{2}^+$	(0.01, 157°) (0.02, -43°)	(0.04, -26°) (0.01, -34°)	(0.04, 156°) (0.01, 33°)	(0.07, 164°) (0.09, 68°)
$N(1720) \frac{3}{2}^+$	(0.12, -32°) (0.13, -28°)	(0.07, 120°) (0.05, 102°)	(0.01, -94°) (0.02, -92°)	(0.01, 118°) (0.03, 104°)
$N(1900) \frac{3}{2}^+$	(0.07, -132°) (0.15, -163°)	(0.04, 53°) (0.08, 28°)	(0.02, -153°) (0.05, -175°)	(0.00, 86°) (0.00, -75°)
$N(1520) \frac{3}{2}^-$	(0.67, -11°) (0.85, -9°)	(0.02, 73°) (0.02, 76°)	(0.03, 134°) (0.03, 127°)	(0.04, -28°) (0.01, 40°)
$N(1700) \frac{3}{2}^-$	(0.09, 68°) (0.05, 146°)	(0.01, 124°) (0.01, -177°)	(0.01, -148°) (0.00, -110°)	(0.01, 87°) (0.00, -156°)
$N(1875) \frac{3}{2}^-$	(0.01, -84°) (0.01, -37°)	(0.00, 56°) (0.00, 112°)	(0.00, -171°) (0.00, -32°)	(0.00, 32°) (0.00, 104°)
$N(1675) \frac{5}{2}^-$	(0.60, -18°) (0.66, -7°)	(0.13, -56°) (0.09, -58°)	(0.01, -59°) (0.02, -9°)	(0.02, -168°) (0.05, -163°)
$N(1680) \frac{5}{2}^+$	(0.81, -20°) (0.79, -21°)	(0.03, 83°) (0.03, 91°)	(0.01, -41°) (0.01, -39°)	(0.01, 139°) (0.00, 114°)
$N(1990) \frac{7}{2}^+$	(0.06, -103°) (0.06, -104°)	(0.02, 125°) (0.02, 140°)	(0.01, -122°) (0.01, -128°)	(0.01, 62°) (0.01, 63°)
$N(2190) \frac{7}{2}^-$	(0.13, -67°) (0.14, -67°)	(0.02, 92°) (0.01, -94°)	(0.02, -98°) (0.01, -112°)	(0.00, -127°) (0.00, -117°)
$N(2250) \frac{9}{2}^-$	(0.12, -112°) (0.19, -128°)	(0.10, -164°) (0.20, -175°)	(0.02, 79°) (0.01, 105°)	(0.03, -161°) (0.07, -170°)
2nd pole $\frac{9}{2}^-$	(0.06, 108°) (0.04, 84°)	(0.06, 123°) (0.03, 106°)	(0.00, 173°) (0.00, 34°)	(0.01, 84°) (0.01, 67°)
$N(2220) \frac{9}{2}^+$	(0.14, -70°) (0.14, -69°)	(0.01, 112°) (0.00, -78°)	(0.01, -86°) (0.01, -89°)	(0.00, -98°) (0.00, -92°)

TABLE VII: The normalized residues of the N^* states for the lower channels, given in the form (NR, θ) , with the phase θ in units of degrees. In each cell, the value of the first (second) row is from fit A (B).

Note that when the energy is below the $\pi\pi N$ threshold and κ corresponds to πN , Eq. (17) is the common definition of the phase shift, namely both $\tilde{\delta}$ and a are real. Specifically the scattering length is extracted from the τ amplitude of Eq. (7),

$$a_\kappa = \lim_{p_\kappa \rightarrow 0} p_\kappa^{-1} \tau_{\kappa\kappa}^{(L=0)}. \quad (18)$$

As already mentioned, the ωN scattering length is very important since it indicates whether the ω meson can form bound states in the nuclear medium. There are two ωN scattering lengths with total spin $S = 1/2, 3/2$. Here we consider the spin-averaged scattering length, which is commonly used in the literature (see e.g. Ref. [68]):

$$\bar{a}_{\omega N} = \frac{1}{3} a_{\omega N} \left(S = \frac{1}{2} \right) + \frac{2}{3} a_{\omega N} \left(S = \frac{3}{2} \right). \quad (19)$$

The results for fits A and B are shown in Tab. XI. Though the real parts of the $S = 1/2$ scattering length are somewhat different, the two results for \bar{a} agree with each other

qualitatively: both of them have a negative real part, indicating that our model, irrespective of the uncertainties, does not support bound states of the ω in nuclear matter. The imaginary parts are relatively smaller, showing weak inelastic effects near the ωN threshold. The values of $\bar{a}_{\omega N}$ here and in the previous studies are plotted in Fig. 10. Our negative real part agrees with all those except for the two studies based on QCD sum rules. Note that in addition to Fig. 10, there are some results on the absolute value of the scattering length, e.g. $|\bar{a}_{\omega N}| = 0.82 \pm 0.03$ fm in Ref. [72], and also $|\bar{a}_{\omega N}| = 0.81 \pm 0.41$ fm from a calculation mentioned therein based on Ref. [138].

Results for the scattering lengths of the lower channels are shown in Tab. XII. The value of πN scattering length is quite similar to Ref. [51] and compatible with the result of the Roy-Steiner analyses in Ref. [139], since the inclusion of a high-lying ωN channel should not affect the physics of πN threshold significantly. However, the scattering lengths of $K\Lambda$ and $K\Sigma$ ($I = 1/2$) have changed

Resonances	πN (Fit A)	πN (Fit B)	$K\Sigma$ (Fit A)	$K\Sigma$ (Fit B)
$\Delta(1620)$ $\frac{1}{2}^-$	(0.47, -107°)	(0.47, -107°)	(0.19, -104°)	(0.18, -105°)
$\Delta(1750)$ $\frac{1}{2}^+$	(0.01, 144°)	—	(0.03, -81°)	—
$\Delta(1910)$ $\frac{1}{2}^+$	(0.20, 150°)	(0.10, 114°)	(0.01, 32°)	(0.01, 75°)
$\Delta(1232)$ $\frac{3}{2}^+$	(1.02, -38°)	(1.01, -40°)	(1.12, -169°)	(1.10, -170°)
$\Delta(1600)$ $\frac{3}{2}^+$	(0.12, -123°)	(0.06, -137°)	(0.14, 12°)	(0.07, 25°)
$\Delta(1920)$ $\frac{3}{2}^+$	(0.09, 88°)	(0.08, 86°)	(0.17, 141°)	(0.16, 139°)
$\Delta(1700)$ $\frac{3}{2}^-$	(0.04, -46°)	(0.05, -26°)	(0.01, 49°)	(0.01, 59°)
$\Delta(1940)$ $\frac{3}{2}^-$	(0.00, -153°)	(0.00, -157°)	(0.03, 22°)	(0.03, 19°)
3rd pole $\frac{3}{2}^-$	—	(0.02, 141°)	—	(0.01, 119°)
$\Delta(1930)$ $\frac{3}{2}^-$	(0.04, -169°)	(0.05, -153°)	(0.00, -4°)	(0.01, -9°)
$\Delta(1905)$ $\frac{3}{2}^+$	(0.01, -104°)	(0.04, -98°)	(0.00, -34°)	(0.00, -37°)
$\Delta(1950)$ $\frac{3}{2}^+$	(0.45, -8°)	(0.45, -8°)	(0.02, -52°)	(0.02, -54°)
$\Delta(2200)$ $\frac{3}{2}^-$	(0.01, -174°)	(0.09, -160°)	(0.00, -6°)	(0.02, 7°)
2nd pole $\frac{3}{2}^-$	—	(0.05, -96°)	—	(0.01, 17°)
$\Delta(2400)$ $\frac{3}{2}^-$	(0.05, -105°)	(0.05, -105°)	(0.00, 16°)	(0.00, 16°)

TABLE VIII: The normalized residues of the Δ states for the lower channels, written in the form (NR, θ) , with the phase θ in units of degrees.

Resonances	πN	ηN	$K\Lambda$	$K\Sigma$
$N(1535)$ $\frac{1}{2}^-$	44.01(40.04)%	51.81(56.80)%	—	—
$N(1650)$ $\frac{1}{2}^-$	46.93(44.98)%	6.49(5.89)%	9.38(9.84)%	—
$N(1440)$ $\frac{1}{2}^+$	39.86(56.63)%	—	—	—
$N(1710)$ $\frac{1}{2}^+$	30.91(84.47)%	85.56(34.49)%	53.29%	4.17%
$N(1880)$ $\frac{1}{2}^+$	1.24(1.89)%	15.04(0.40)%	12.53(0.98)%	38.88(41.85)%
$N(1720)$ $\frac{3}{2}^+$	12.15(13.32)%	3.64(1.55)%	0.14(0.34)%	—
$N(1900)$ $\frac{3}{2}^+$	6.92(15.27)%	2.09(4.09)%	0.37(1.62)%	0.03(0.18)%
$N(1520)$ $\frac{3}{2}^-$	66.81(84.65)%	0.04(0.06)%	—	—
$N(1700)$ $\frac{3}{2}^-$	8.72(4.99)%	—	—	—
$N(1875)$ $\frac{3}{2}^-$	1.36(1.31)%	0.02(0.02)%	0.00(0.00)%	0.01(0.00)%
$N(1675)$ $\frac{3}{2}^-$	59.73(65.74)%	2.69(1.32)%	0.03(0.07)%	—
$N(1680)$ $\frac{3}{2}^+$	81.17(79.44)%	0.08(0.08)%	0.01(0.00)%	—
$N(1990)$ $\frac{3}{2}^+$	5.56(5.79)%	0.58(0.42)%	0.10(0.18)%	0.37(0.32)%
$N(2190)$ $\frac{3}{2}^-$	12.90(13.69)%	0.21(0.05)%	0.17(0.08)%	0.00(0.00)%
$N(2250)$ $\frac{3}{2}^-$	12.20(18.69)%	7.58(20.42)%	0.24(0.04)%	0.97(2.91)%
2nd pole $\frac{3}{2}^-$	5.58(3.67)%	5.51(3.08)%	0.01(0.00)%	0.35(0.21)%
$N(2220)$ $\frac{3}{2}^+$	13.57(13.98)%	0.03(0.01)%	0.11(0.07)%	0.00(0.00)%

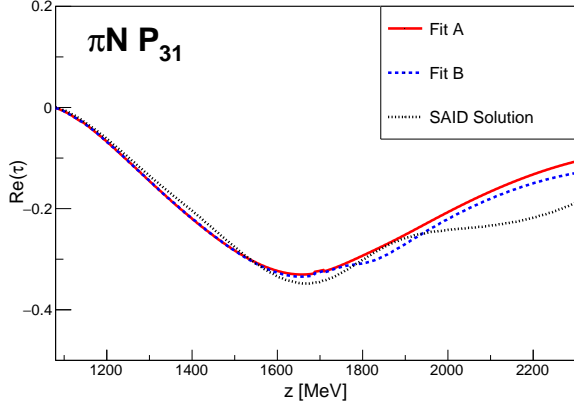
TABLE IX: The branching ratios (in percent) of the N^* states to the lower physical channels, defined by Eq. (14). The values outside (inside) the brackets are from fit A (B).

considerably compared with the results in Ref. [51]. This discrepancy possibly stems from the lack of precision of the corresponding near-threshold data points. The error-bars of the near-threshold differential cross sections in the $\pi N \rightarrow K\Lambda, K\Sigma$ reactions are rather large.

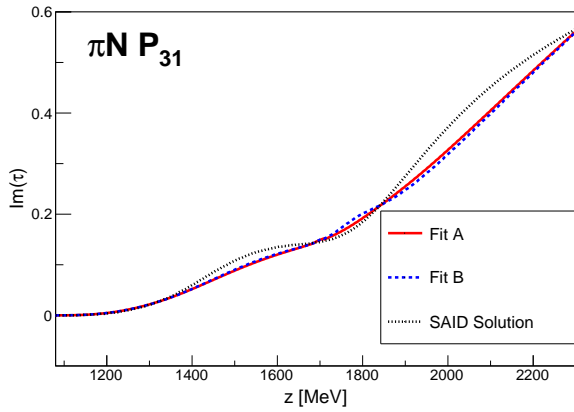
V. CONCLUSION AND OUTLOOK

In this paper we have performed a refined investigation on pion-induced meson-baryon scattering reactions, using a sophisticated coupled-channel approach (the Jülich-

Bonn model). The model includes t - and u -channel exchange diagrams and s -channel genuine states in addition to phenomenological contact terms, taking into account the πN , $\pi\pi N$ (effectively parameterized by $\pi\Delta$, σN and ρN), ηN , $K\Lambda$ and $K\Sigma$ channels with ωN newly included. This model covers the energy region from the πN threshold up to 2.3 GeV, and fits are done based on all available data. The model-dependence is estimated by comparing two different fit scenarios. After the calculation of the amplitudes and extraction of the resonance poles, the N^* and Δ resonance spectra are reanalysed, and the following conclusions can be drawn:



(a) The real part.



(b) The imaginary part.

FIG. 9: Fit results of P_{31} πN elastic τ amplitude. The SAID solution is from Ref. [30] (energy-dependent solution). We do not need a narrow $\Delta(1910)$ pole in both of the two fit scenarios.

- While the well established N^* states like $N(1535) \frac{1}{2}^-$, $N(1650) \frac{1}{2}^-$, etc., always remain nearly unchanged, some resonances in higher partial waves are found to be stable. The main discrepancy of the two fit scenarios is the dynamical structure of the P_{11} wave.
- As for the Δ states, even if ωN does not couple to them, the results are also refined by the new global fits. Specifically, the $\Delta(1910) \frac{1}{2}^+$ in our model is rather broad.
- The ωN channel mainly couples to three low-lying states in this model, $N(1535) \frac{1}{2}^-$, $N(1710) \frac{1}{2}^+$ and $N(1680) \frac{5}{2}^+$. The higher resonances do not show markable couplings to the ωN channel, with the $N(2250) \frac{9}{2}^-$ being the most important one.
- The spin-averaged scattering length of ωN is calculated, resulting in a negative real part. In fit A it is

Resonances	πN	$K\Sigma$
$\Delta(1620) \frac{1}{2}^-$	47.13(46.92)%	—
$\Delta(1750) \frac{1}{2}^+$	1.2%	5.6%
$\Delta(1910) \frac{1}{2}^+$	19.75(9.93)%	0.06(0.03)%
$\Delta(1232) \frac{3}{2}^+$	101.86(101.39)%	—
$\Delta(1600) \frac{1}{2}^+$	11.70(6.44)%	—
$\Delta(1920) \frac{1}{2}^+$	9.17(8.04)%	32.08(32.72)%
$\Delta(1700) \frac{1}{2}^-$	4.46(5.06)%	0.36(0.33)%
$\Delta(1940) \frac{1}{2}^-$	0.24(0.41)%	28.86(28.17)%
3rd pole	(2.44%)	—
$\Delta(1930) \frac{1}{2}^-$	3.91(5.20)%	0.03(0.07)%
$\Delta(1905) \frac{1}{2}^+$	1.33(3.98)%	0.00(0.00)%
$\Delta(1950) \frac{1}{2}^+$	45.06(45.48)%	0.12(0.12)%
$\Delta(2200) \frac{1}{2}^-$	0.79(8.75)%	0.01(0.26)%
2nd pole	(4.80%)	(0.28%)
$\Delta(2400) \frac{3}{2}^-$	5.17(5.26)%	0.01(0.01)%

TABLE X: The branching ratios (in percent) of the Δ states to the lower physical channels, defined by Eq. (14). The values outside (inside) the brackets are from fit A (B).

$(-0.24 + 0.05i)$ fm and in fit B $(-0.21 + 0.05i)$ fm. This, in agreement with most other studies, does not support bound states of the ω meson in nuclear matter.

There are two main directions for future studies. On the one hand, building on the framework of Refs. [56, 135], we plan to extend the current work to ω photoproduction, profiting from the large amount of high-quality data that will be of high importance to further refine the ωN resonance parameters. On the other hand, the output of this work can be directly used as the input for e.g. studying the in-medium behavior of the ω meson, or investigating the possible hadronic molecules [140] among the N^* and Δ resonances. Last, this model can also be employed to check the possible structures below the πN threshold [141–147].

ACKNOWLEDGEMENTS

We would like to thank Zhi-Hui Guo, Johann Haidenbauer and Fei Huang for helpful instructions on consistency checks of the theoretical framework, and Michael Döring for useful discussions. The authors gratefully acknowledge the computing time granted by the JARA Vergabegremium and provided on the JARA Partition part of the supercomputer JURECA [129] at Forschungszentrum Jülich. This work is supported by the NSFC and the Deutsche Forschungsgemeinschaft (DFG, German Research Foundation) through the funds provided to the Sino-German Collaborative Research Center TRR110 “Symmetries and the Emergence of Structure in QCD” (NSFC Grant No. 12070131001, DFG Project-ID

Fit	$a_{\omega N}(S = \frac{1}{2})$	$a_{\omega N}(S = \frac{3}{2})$	$\bar{a}_{\omega N}$
A	$-0.13 + 0.11i$	$-0.31 + 0.01i$	$-0.24 + 0.05i$
B	$-0.04 + 0.13i$	$-0.29 + 0.01i$	$-0.21 + 0.05i$

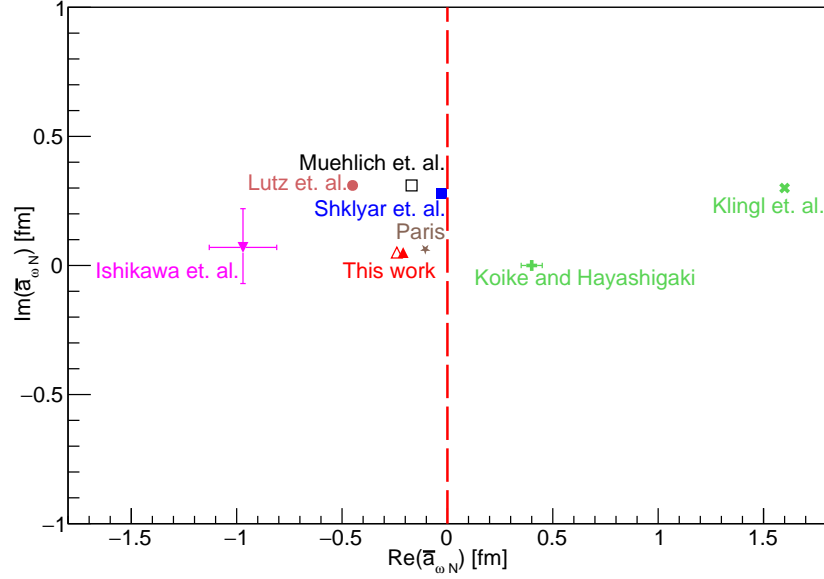
TABLE XI: The scattering lengths of ωN channel in units of fms.

FIG. 10: A summary of the spin-averaged ωN scattering length. The result from fit A (B) is denoted by the empty (filled) red triangle. The relevant references are: Koike and Hayashigaki [68], Klingl et. al. [70], Lutz et al. [34], Shklyar et al. [38], Muehlich et al. [71], Paris [48] and Ishikawa et al. [74].

Result	$a_{\pi N, I = \frac{1}{2}}(\frac{3}{2})$	$a_{\eta N}$	$a_{K\Lambda}$	$a_{K\Sigma, I = \frac{1}{2}}(\frac{3}{2})$
Fit A	$0.25(-0.16)$	$0.51 + 0.20i$	$-0.15 + 0.05i$	$-0.01(-0.39) + 0.30(0.02)i$
Fit B	$0.25(-0.16)$	$0.57 + 0.22i$	$-0.15 + 0.04i$	$-0.07(-0.39) + 0.29(0.01)i$
Fit A of Ref. [51]	$0.25(-0.16)$	$0.49 + 0.24i$	$0.04 + 0.04i$	$0.36(-0.30) + 0.15(0.04)i$
Fit B of Ref. [51]	$0.29(-0.16)$	$0.55 + 0.24i$	$0.04 + 0.03i$	$0.32(-0.30) + 0.14(0.05)i$
Ref. [139]	$0.257 \pm 0.005(-0.112 \pm 0.004)$	—	—	—

TABLE XII: The scattering lengths of the lower channels in units of fms.

196253076-TRR 110) and by the National Natural Science Foundation of China under Grants No. 12175239 and the National Key R&D Program of China under Contract No. 2020YFA0406400. Further support by the CAS through a President's International Fellowship Initiative (PIFI) (Grant No. 2018DM0034) and by the VolkswagenStiftung (Grant No. 93562) is acknowledged.

Appendix A: Observables of the omega-nucleon channel

The expression of the differential cross section for either $\pi^- p \rightarrow \omega n$ or $\pi^+ n \rightarrow \omega p$ is:

$$\begin{aligned}
\frac{d\bar{\sigma}}{d\Omega} = & \frac{2}{3p_i^2} \left[\left| \sum_J (2J+1) \tau_{++0}^J d_{1/2,1/2}^J(\theta) \right|^2 + \left| \sum_J (2J+1) \tau_{+-0}^J d_{1/2,-1/2}^J(\theta) \right|^2 \right. \\
& + \left| \sum_J (2J+1) \tau_{+--}^J d_{1/2,1/2}^J(\theta) \right|^2 + \left| \sum_J (2J+1) \tau_{+++}^J d_{1/2,-1/2}^J(\theta) \right|^2 \\
& \left. + \left| \sum_J (2J+1) \tau_{++-}^J d_{1/2,3/2}^J(\theta) \right|^2 + \left| \sum_J (2J+1) \tau_{+-+}^J d_{1/2,-3/2}^J(\theta) \right|^2 \right], \quad (A1)
\end{aligned}$$

where the initial spins are averaged and the final ones are summed, the d^J 's are Wigner d -functions (with the scattering angle θ as the argument) and $\tau_{\lambda_1 \lambda_3 \lambda_4}^J$ are the amplitudes of Eq. (7) written in the helicity basis (total isospin $I = 1/2$), with λ_1, λ_3 and λ_4 being the helicities

of initial nucleon, final nucleon and final ω , respectively ("±" stands for $\lambda = \pm \frac{1}{2}$ or ± 1). The relation between the τ amplitudes in Eq. (7) (JLS basis) and in Eq. (A1) (helicity basis) is:

$$\begin{pmatrix} \tau_{++0}^J \\ \tau_{+-0}^J \\ \tau_{+--}^J \\ \tau_{+++}^J \\ \tau_{++-}^J \\ \tau_{+-+}^J \end{pmatrix} = \frac{1}{12} \begin{pmatrix} 2\sqrt{3} & -3\sqrt{\frac{2J-1}{J}} & \sqrt{\frac{6J+9}{J}} & 2\sqrt{3} & 3\sqrt{\frac{2J+3}{J+1}} & -\sqrt{\frac{6J-3}{J+1}} \\ 2\sqrt{3} & -3\sqrt{\frac{2J-1}{J}} & \sqrt{\frac{6J+9}{J}} & -2\sqrt{3} & -3\sqrt{\frac{2J+3}{J+1}} & \sqrt{\frac{6J-3}{J+1}} \\ -2\sqrt{6} & -3\sqrt{\frac{2J-1}{2J}} & \sqrt{\frac{6J+9}{2J}} & -2\sqrt{6} & 3\sqrt{\frac{2J+3}{2J+2}} & -\sqrt{\frac{6J-3}{2J+2}} \\ -2\sqrt{6} & -3\sqrt{\frac{2J-1}{2J}} & \sqrt{\frac{6J+9}{2J}} & 2\sqrt{6} & -3\sqrt{\frac{2J+3}{2J+2}} & \sqrt{\frac{6J-3}{2J+2}} \\ 0 & -3\sqrt{\frac{2J+3}{2J}} & -3\sqrt{\frac{6J-3}{2J}} & 0 & -3\sqrt{\frac{2J-1}{2J+2}} & -3\sqrt{\frac{6J+9}{2J+2}} \\ 0 & -3\sqrt{\frac{2J+3}{2J}} & -3\sqrt{\frac{6J-3}{2J}} & 0 & 3\sqrt{\frac{2J-1}{2J+2}} & 3\sqrt{\frac{6J+9}{2J+2}} \end{pmatrix} \begin{pmatrix} \tau_{p_1 p_1 S_1}^J \\ \tau_{p_1 m_3 S_3}^J \\ \tau_{p_1 p_1 S_3}^J \\ \tau_{m_1 m_1 S_1}^J \\ \tau_{m_1 p_3 S_3}^J \\ \tau_{m_1 m_1 S_3}^J \end{pmatrix}, \quad (A2)$$

using the abbreviations

$$\begin{pmatrix} \tau_{p_1 p_1 S_1}^J \\ \tau_{p_1 m_3 S_3}^J \\ \tau_{p_1 p_1 S_3}^J \\ \tau_{m_1 m_1 S_1}^J \\ \tau_{m_1 p_3 S_3}^J \\ \tau_{m_1 m_1 S_3}^J \end{pmatrix} \equiv \begin{pmatrix} \tau^J \left(L_i = J + \frac{1}{2}, L_f = J + \frac{1}{2}, S_f = \frac{1}{2} \right) \\ \tau^J \left(L_i = J + \frac{1}{2}, L_f = J - \frac{3}{2}, S_f = \frac{3}{2} \right) \\ \tau^J \left(L_i = J + \frac{1}{2}, L_f = J + \frac{1}{2}, S_f = \frac{3}{2} \right) \\ \tau^J \left(L_i = J - \frac{1}{2}, L_f = J - \frac{1}{2}, S_f = \frac{1}{2} \right) \\ \tau^J \left(L_i = J - \frac{1}{2}, L_f = J + \frac{3}{2}, S_f = \frac{3}{2} \right) \\ \tau^J \left(L_i = J - \frac{1}{2}, L_f = J - \frac{1}{2}, S_f = \frac{3}{2} \right) \end{pmatrix}. \quad (A3)$$

After integrating over the angular dependence, the total cross section for either $\pi^- p \rightarrow \omega n$ or $\pi^+ n \rightarrow \omega p$ is:

$$\begin{aligned}
\bar{\sigma} = & \frac{8\pi}{3p_i^2} \sum_J (2J+1) \left(|\tau_{++0}^J|^2 + |\tau_{+-0}^J|^2 + |\tau_{+--}^J|^2 \right. \\
& \left. + |\tau_{+++}^J|^2 + |\tau_{++-}^J|^2 + |\tau_{+-+}^J|^2 \right). \quad (A4)
\end{aligned}$$

Appendix B: Partial wave amplitudes of $\pi N \rightarrow \omega N$

The partial wave amplitudes of $\pi N \rightarrow \omega N$ in this work do not show significant structures, and depend not much on the two different fit solutions especially when the energy is close to the ωN threshold. For partial waves with

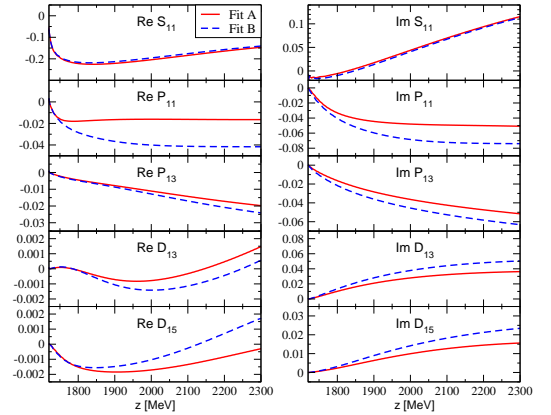


FIG. 11: Partial wave amplitudes with $L_{\pi N} \leq 2$, in the sub-channel (1) of ωN : $|J - L_{\omega N}| = \frac{1}{2}$, $S_{\omega N} = \frac{1}{2}$. The notation $L_{2I,2J}$ is for the initial πN system.

(πN) orbital angular momentum $L \leq 2$, see Figs. 11, 12 and 13, for $L \geq 3$ see Figs. 14, 15 and 16. The magnitude of F_{15} amplitude in sub-channel (3) is relatively large, since the coupling of ωN to $N(1680) \frac{5}{2}^+$ is rather strong. Note that the $N^*(1680)$ is only a P -wave resonance for ωN .

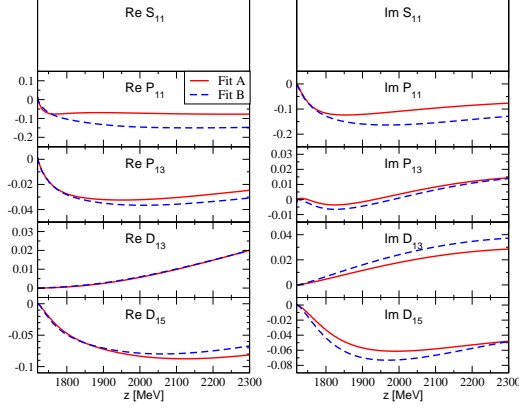


FIG. 12: Partial wave amplitudes with $L_{\pi N} \leq 2$, in the sub-channel (2) of ωN : $|J - L_{\omega N}| = \frac{1}{2}$, $S_{\omega N} = \frac{3}{2}$. The notation $L_{2I,2J}$ is for the initial πN system.

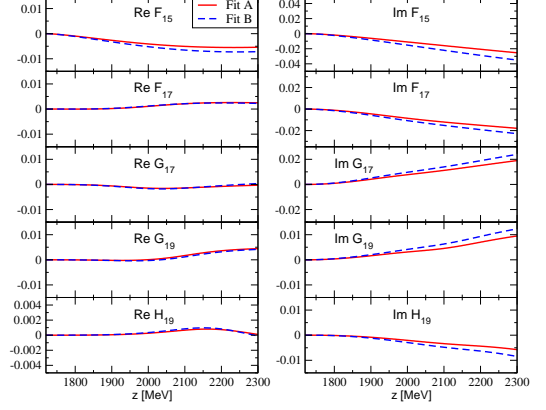


FIG. 14: Partial wave amplitudes with $L_{\pi N} \geq 3$, in the sub-channel (1) of ωN : $|J - L_{\omega N}| = \frac{1}{2}$, $S_{\omega N} = \frac{1}{2}$. The notation $L_{2I,2J}$ is for the initial πN system.

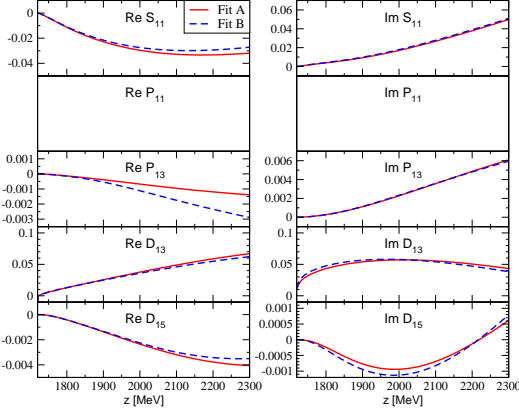


FIG. 13: Partial wave amplitudes with $L_{\pi N} \leq 2$, in the sub-channel (3) of ωN : $|J - L_{\omega N}| = \frac{3}{2}$, $S_{\omega N} = \frac{3}{2}$. The notation $L_{2I,2J}$ is for the initial πN system.

Appendix C: Couplings of the resonances to effective three-body channels

In this section the complex couplings g_μ to the effective three-body channels (σN excluded) are given as:

$$\tilde{T}_{\mu\nu} \sim \frac{g_\mu g_\nu}{z - z_0} + \dots; \quad (C1)$$

where g_μ is related to R_μ by Eq. (7). The results are shown for the N^* states in Tab. XIII and for the Δ states in Tab. XIV. In this model we do not consider the couplings of σN to the resonances.

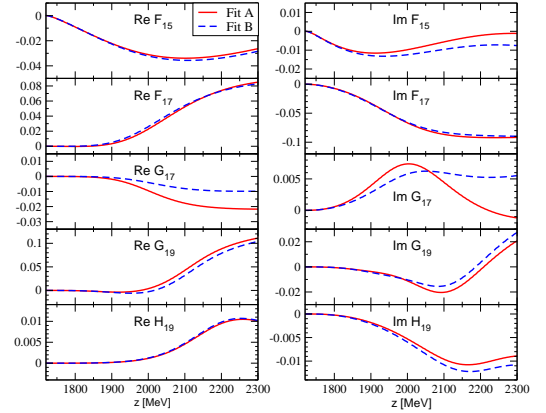


FIG. 15: Partial wave amplitudes with $L_{\pi N} \geq 3$, in the sub-channel (2) of ωN : $|J - L_{\omega N}| = \frac{1}{2}$, $S_{\omega N} = \frac{3}{2}$. The notation $L_{2I,2J}$ is for the initial πN system.

Resonances	$\pi\Delta$ (1)	$\pi\Delta$ (2)	ρN (1)	ρN (2)	ρN (3)
$N(1535) \frac{1}{2}^-$	0	$-6.3 + 4.2i$ ($-6.0 + 4.4i$)	$-5.4 - 1.2i$ ($-4.9 - 0.8i$)	0	$-0.2 - 0.4i$ ($-0.2 - 0.3i$)
$N(1650) \frac{1}{2}^-$	0	$4.1 + 4.1i$ ($5.1 + 3.3i$)	$-2.2 + 16.1i$ ($-1.5 + 15.5i$)	0	$0.4 + 2.6i$ ($0.5 + 2.6i$)
$N(1440) \frac{1}{2}^+$	$-6.7 + 4.3i$ ($-7.2 + 4.4i$)	0	$1.1 + 3.1i$ ($-1.4 + 5.6i$)	$3.6 - 3.2i$ ($4.3 - 0.7i$)	0
$N(1710) \frac{1}{2}^+$	$8.6 + 3.7i$ ($11.6 - 5.8i$)	0	$-1.4 + 0.1i$ ($3.5 + 5.0i$)	$1.5 - 1.0i$ ($4.9 - 4.4i$)	0
$N(1880) \frac{1}{2}^+$	$2.8 + 0.2i$ ($1.1 + 0.5i$)	0	$0.1 + 1.0i$ ($-0.7 + 0.6i$)	$0.2 - 0.2i$ ($0.5 + 0.0i$)	0
$N(1720) \frac{3}{2}^+$	$14.4 + 2.7i$ ($16.5 + 3.3i$)	$-0.6 - 0.1i$ ($-0.6 - 0.2i$)	$-1.3 - 1.0i$ ($-1.5 - 1.2i$)	$-2.5 + 13.8i$ ($-2.3 + 14.9i$)	$1.0 - 0.4i$ ($1.1 - 0.5i$)
$N(1900) \frac{3}{2}^+$	$-9.1 + 11.3i$ ($-7.7 + 20.7i$)	$-0.1 - 0.2i$ ($-2.7 + 1.2i$)	$1.6 - 0.4i$ ($2.3 - 0.7i$)	$2.6 + 4.2i$ ($5.8 + 5.0i$)	$0.3 - 1.8i$ ($0.4 - 1.1i$)
$N(1520) \frac{3}{2}^-$	$-0.1 + 1.4i$ ($-0.1 + 1.7i$)	$-13.2 - 2.5i$ ($-14.0 - 4.0i$)	$-1.8 + 1.2i$ ($-2.1 + 1.2i$)	$-1.7 + 0.2i$ ($-1.9 + 0.2i$)	$2.4 - 24.6i$ ($3.0 - 28.0i$)
$N(1700) \frac{3}{2}^-$	$0.3 + 1.6i$ ($1.0 - 1.0i$)	$16.0 - 15.1i$ ($-21.8 + 14.2i$)	$-2.4 - 1.7i$ ($3.7 + 2.5i$)	$0.9 + 0.5i$ ($-1.1 + 3.9i$)	$-1.7 + 0.0i$ ($-3.1 - 8.9i$)
$N(1875) \frac{3}{2}^-$	$-12.1 + 10.1i$ ($-13.5 + 7.1i$)	$1.9 - 0.2i$ ($2.7 + 0.7i$)	$-2.4 - 0.2i$ ($-2.1 - 1.1i$)	$0.9 - 1.2i$ ($1.1 - 1.2i$)	$0.5 + 0.9i$ ($0.3 + 0.6i$)
$N(1675) \frac{5}{2}^-$	$-12.9 + 3.2i$ ($-12.5 + 1.8i$)	$0.3 - 0.0i$ ($0.3 + 0.0i$)	$1.5 + 2.3i$ ($1.0 + 2.2i$)	$-4.3 + 0.6i$ ($-4.4 - 0.1i$)	$-1.0 - 0.2i$ ($-1.1 - 0.2i$)
$N(1680) \frac{5}{2}^+$	$-0.2 - 0.1i$ ($-0.2 - 0.0i$)	$-6.3 + 1.4i$ ($-6.5 + 1.2i$)	$-1.2 + 1.0i$ ($-1.2 + 1.0i$)	$-0.7 + 0.5i$ ($-0.7 + 0.4i$)	$0.0 - 4.4i$ ($0.1 - 4.4i$)
$N(1990) \frac{7}{2}^+$	$-5.0 + 5.0i$ ($-5.3 + 5.1i$)	$-0.0 - 0.9i$ ($-0.3 - 1.2i$)	$1.1 + 0.6i$ ($1.2 + 0.6i$)	$6.1 + 4.0i$ ($6.3 + 4.1i$)	$0.1 - 0.0i$ ($0.1 - 0.1i$)
$N(2190) \frac{7}{2}^-$	$0.3 - 1.0i$ ($0.3 - 1.0i$)	$-6.7 + 6.6i$ ($-6.7 + 6.9i$)	$-0.2 - 0.1i$ ($-0.3 - 0.1i$)	$-0.4 - 0.9i$ ($-0.5 - 1.0i$)	$-3.1 - 4.9i$ ($-3.2 - 5.3i$)
$N(2250) \frac{9}{2}^-$	$-7.1 + 5.4i$ ($-8.5 + 6.5i$)	$0.7 - 0.5i$ ($0.7 - 0.6i$)	$1.1 + 0.1i$ ($1.0 + 0.3i$)	$-6.2 - 3.0i$ ($-7.5 - 3.9i$)	$-0.9 + 0.3i$ ($-0.9 + 0.5i$)
2nd pole $\frac{9}{2}^-$	$-7.3 - 0.1i$ ($-6.7 + 0.8i$)	$0.5 - 0.1i$ ($0.4 - 0.0i$)	$-0.5 + 0.5i$ ($0.3 + 0.7i$)	$-4.9 - 0.8i$ ($-4.2 - 1.4i$)	$0.3 + 0.3i$ ($-0.4 - 0.1i$)
$N(2220) \frac{9}{2}^+$	$-0.2 + 0.4i$ ($-0.3 + 0.4i$)	$10.3 - 5.3i$ ($10.4 - 5.2i$)	$-0.9 - 1.5i$ ($-1.0 - 1.5i$)	$-0.5 - 1.8i$ ($-0.5 - 1.8i$)	$2.6 + 0.3i$ ($2.6 + 0.3i$)

TABLE XIII: The complex couplings of N^* states to the effective three-body channels (in units of $10^{-3}\sqrt{\text{MeV}}$), defined by Eq. (C1). The values outside (inside) the brackets are from fit A (B). $\pi\Delta$ (1,2) stand for $|J-L| = \frac{1}{2}, \frac{3}{2}$, respectively; while the three sub-channels of ρN are: (1) $|J-L| = \frac{1}{2}, S = \frac{1}{2}$; (2) $|J-L| = \frac{1}{2}, S = \frac{3}{2}$; (3) $|J-L| = \frac{3}{2}, S = \frac{3}{2}$.

Resonances	$\pi\Delta$ (1)	$\pi\Delta$ (2)	ρN (1)	ρN (2)	ρN (3)
$\Delta(1620) \frac{1}{2}^-$	0	$-10.1 + 3.4i$ ($-10.1 + 3.3i$)	$2.5 + 7.6i$ ($2.4 + 7.2i$)	0	$0.7 + 0.9i$ ($0.7 + 0.9i$)
$\Delta(1750) \frac{1}{2}^+$	$-1.2 - 0.7i$	0	$0.5 + 1.9i$	$0.6 + 0.6i$	0
$\Delta(1910) \frac{1}{2}^+$	$-15.3 + 12.8i$ ($5.6 - 11.1i$)	0	$-1.7 - 1.2i$ ($1.4 + 0.0i$)	$-1.4 - 4.1i$ ($3.3 + 0.8i$)	0
$\Delta(1232) \frac{3}{2}^+$	$54.8 + 20.0i$ ($59.5 + 23.9i$)	$-4.3 + 2.9i$ ($-5.8 + 2.2i$)	$-8.1 - 9.3i$ ($-7.9 - 9.0i$)	$1.3 - 2.7i$ ($0.4 - 4.3i$)	$6.7 + 2.2i$ ($6.4 + 1.8i$)
$\Delta(1600) \frac{3}{2}^+$	$-16.4 + 6.6i$ ($-10.4 + 5.8i$)	$0.5 - 0.0i$ ($0.3 - 0.0i$)	$7.5 + 2.4i$ ($4.8 + 0.7i$)	$7.4 + 5.4i$ ($4.7 + 3.0i$)	$-2.4 + 0.2i$ ($-1.5 + 0.8i$)
$\Delta(1920) \frac{3}{2}^+$	$3.0 - 0.4i$ ($3.5 - 0.0i$)	$-1.1 - 0.7i$ ($-1.1 - 0.6i$)	$0.2 + 2.3i$ ($0.4 + 2.0i$)	$1.0 + 0.9i$ ($1.2 + 0.9i$)	$-1.5 - 0.1i$ ($-1.4 - 0.1i$)
$\Delta(1700) \frac{3}{2}^-$	$1.9 + 2.9i$ ($2.0 + 2.6i$)	$-19.1 + 4.3i$ ($-20.1 + 4.2i$)	$0.3 - 1.7i$ ($0.2 - 2.1i$)	$2.2 - 0.2i$ ($2.3 - 0.4i$)	$7.2 + 7.6i$ ($7.6 + 8.1i$)
$\Delta(1940) \frac{3}{2}^-$	$-2.1 + 0.5i$ ($-1.9 + 0.4i$)	$0.8 - 2.8i$ ($0.7 - 2.0i$)	$-0.3 + 0.4i$ ($-0.3 + 0.3i$)	$-0.0 + 0.3i$ ($-0.0 + 0.2i$)	$-1.3 + 0.1i$ ($-0.8 - 0.1i$)
3rd pole $\frac{3}{2}^-$	$(1.6 + 1.6i)$	$(-13.0 + 14.9i)$	$(-3.8 - 1.1i)$	$(-5.4 + 0.1i)$	$(3.9 - 8.1i)$
$\Delta(1930) \frac{5}{2}^-$	$-8.6 + 9.7i$ ($-9.7 + 11.8i$)	$-0.1 - 0.6i$ ($0.0 - 0.5i$)	$2.5 - 1.1i$ ($3.3 - 0.4i$)	$1.0 - 0.2i$ ($2.1 + 0.6i$)	$1.0 + 0.2i$ ($0.3 + 1.1i$)
$\Delta(1905) \frac{5}{2}^+$	$-0.2 - 0.1i$ ($-0.2 - 0.0i$)	$-1.4 + 1.4i$ ($-1.6 + 2.5i$)	$-0.3 - 0.0i$ ($-0.0 + 0.2i$)	$0.3 + 0.5i$ ($0.7 + 0.9i$)	$2.7 + 4.7i$ ($5.3 + 7.7i$)
$\Delta(1950) \frac{7}{2}^+$	$-6.4 + 1.3i$ ($-6.5 + 1.3i$)	$0.2 - 0.6i$ ($0.2 - 0.5i$)	$2.1 + 1.8i$ ($2.1 + 1.8i$)	$4.4 + 5.1i$ ($4.5 + 5.1i$)	$-0.3 + 0.5i$ ($-0.3 + 0.4i$)
$\Delta(2200) \frac{7}{2}^-$	$0.0 + 0.7i$ ($0.8 + 2.4i$)	$3.4 + 0.5i$ ($4.1 + 2.0i$)	$0.5 - 2.2i$ ($0.9 - 2.9i$)	$0.8 - 1.9i$ ($2.3 - 3.3i$)	$1.3 + 2.0i$ ($4.4 + 3.4i$)
2nd pole $\frac{7}{2}^-$	$(-1.2 + 0.3i)$	$(-7.6 + 6.2i)$	$(1.9 + 1.5i)$	$(3.4 + 2.0i)$	$(3.9 + 4.8i)$
$\Delta(2400) \frac{9}{2}^-$	$7.4 - 9.5i$ ($7.4 - 9.5i$)	$-0.0 + 0.9i$ ($-0.0 + 0.9i$)	$-1.9 + 1.0i$ ($-2.0 + 0.9i$)	$0.6 + 1.1i$ ($0.6 + 1.1i$)	$-0.0 - 0.2i$ ($-0.0 - 0.2i$)

TABLE XIV: The complex couplings of Δ states to the effective three-body channels (in units of $10^{-3}\sqrt{\text{MeV}}$), defined by Eq. (C1). The values outside (inside) the brackets are from fit A (B). $\pi\Delta$ (1,2) stand for $|J-L| = \frac{1}{2}, \frac{3}{2}$, respectively; while the three sub-channels of ρN are: (1) $|J-L| = \frac{1}{2}, S = \frac{1}{2}$; (2) $|J-L| = \frac{1}{2}, S = \frac{3}{2}$; (3) $|J-L| = \frac{3}{2}, S = \frac{3}{2}$.

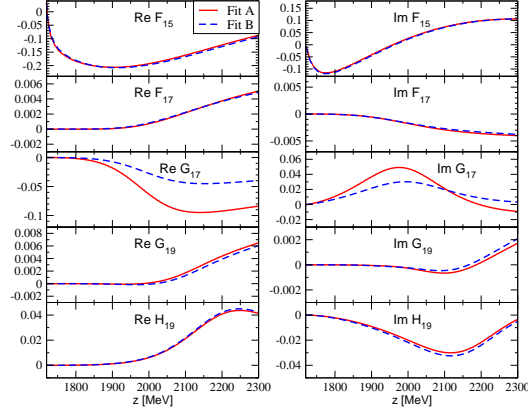


FIG. 16: Partial wave amplitudes with $L_{\pi N} \geq 3$, in the sub-channel (3) of ωN : $|J - L_{\omega N}| = \frac{3}{2}$, $S_{\omega N} = \frac{3}{2}$. The notation $L_{2I,2J}$ is for the initial πN system.

-
- [1] S. Weinberg, Phys. Rev. Lett. **18**, 188 (1967).
 - [2] S. Weinberg, Phys. Rev. **166**, 1568 (1968).
 - [3] S. R. Coleman, J. Wess, and B. Zumino, Phys. Rev. **177**, 2239 (1969).
 - [4] C. G. Callan, Jr., S. R. Coleman, J. Wess, and B. Zumino, Phys. Rev. **177**, 2247 (1969).
 - [5] E. E. Jenkins and A. V. Manohar, Phys. Lett. B **255**, 558 (1991).
 - [6] U.-G. Meißner, Rept. Prog. Phys. **56**, 903 (1993), hep-ph/9302247.
 - [7] H. Leutwyler, Annals Phys. **235**, 165 (1994), hep-ph/9311274.
 - [8] G. Ecker, Prog. Part. Nucl. Phys. **35**, 1 (1995), hep-ph/9501357.
 - [9] V. Bernard, N. Kaiser, and U.-G. Meißner, Int. J. Mod. Phys. E **4**, 193 (1995), hep-ph/9501384.
 - [10] S. Scherer, Adv. Nucl. Phys. **27**, 277 (2003), hep-ph/0210398.
 - [11] V. Bernard and U.-G. Meißner, Ann. Rev. Nucl. Part. Sci. **57**, 33 (2007), hep-ph/0611231.
 - [12] V. Bernard, N. Kaiser, and U.-G. Meißner, Phys. Lett. B **309**, 421 (1993), hep-ph/9304275.
 - [13] M. Mojziz, Eur. Phys. J. C **2**, 181 (1998), hep-ph/9704415.
 - [14] N. Fettes, U.-G. Meißner, and S. Steininger, Nucl. Phys. A **640**, 199 (1998), hep-ph/9803266.
 - [15] T. Becher and H. Leutwyler, Eur. Phys. J. C **9**, 643 (1999), hep-ph/9901384.
 - [16] N. Fettes and U.-G. Meißner, Nucl. Phys. A **693**, 693 (2001), hep-ph/0101030.
 - [17] M. Hoferichter, B. Kubis, and U.-G. Meißner, Nucl. Phys. A **833**, 18 (2010), 0909.4390.
 - [18] J. M. Alarcon, J. Martin Camalich, and J. A. Oller, Annals Phys. **336**, 413 (2013), 1210.4450.
 - [19] Y.-H. Chen, D.-L. Yao, and H.-Q. Zheng, Phys. Rev. D **87**, 054019 (2013), 1212.1893.
 - [20] E. E. Jenkins and A. V. Manohar, Phys. Lett. B **259**, 353 (1991).
 - [21] T. R. Hemmert, B. R. Holstein, and J. Kambor, J. Phys. G **24**, 1831 (1998), hep-ph/9712496.
 - [22] S. R. Beane and U. van Kolck, J. Phys. G **31**, 921 (2005), nucl-th/0212039.
 - [23] V. Pascalutsa, M. Vanderhaeghen, and S. N. Yang, Phys. Rept. **437**, 125 (2007), hep-ph/0609004.
 - [24] B. Borasoy, P. C. Bruns, U.-G. Meißner, and R. Lewis, Phys. Lett. B **641**, 294 (2006), hep-lat/0608001.
 - [25] D.-L. Yao *et al.*, JHEP **05**, 038 (2016), 1603.03638.
 - [26] D. Siemens *et al.*, Phys. Rev. C **94**, 014620 (2016), 1602.02640.
 - [27] J. Gegelia, U.-G. Meißner, and D.-L. Yao, Phys. Lett. B **760**, 736 (2016), 1606.04873.
 - [28] D. Siemens *et al.*, Phys. Lett. B **770**, 27 (2017), 1610.08978.
 - [29] D. Siemens *et al.*, Phys. Rev. C **96**, 055205 (2017), 1704.08988.
 - [30] R. A. Arndt, W. J. Briscoe, I. I. Strakovsky, and R. L. Workman, Phys. Rev. C **74**, 045205 (2006), nucl-th/0605082.
 - [31] R. L. Workman, R. A. Arndt, and M. W. Paris, Phys. Rev. C **79**, 038201 (2009), 0808.2176.
 - [32] R. Koniuk and N. Isgur, Phys. Rev. Lett. **44**, 845 (1980).
 - [33] P. C. Bruns, M. Mai, and U.-G. Meißner, Phys. Lett. B **697**, 254 (2011), 1012.2233.
 - [34] M. F. M. Lutz, G. Wolf, and B. Friman, Nucl. Phys. A **706**, 431 (2002), nucl-th/0112052, [Erratum: Nucl.Phys.A 765, 431–496 (2006), Erratum: Nucl.Phys.A 765, 495–495 (2006)].
 - [35] G. Penner and U. Mosel, Phys. Rev. C **65**, 055202 (2002), nucl-th/0111023, [Erratum: Phys.Rev.C 65, 059901 (2002)].
 - [36] G. Penner and U. Mosel, Phys. Rev. C **66**, 055211 (2002), nucl-th/0207066.
 - [37] G. Penner and U. Mosel, Phys. Rev. C **66**, 055212 (2002), nucl-th/0207069.
 - [38] V. Shklyar, H. Lenske, U. Mosel, and G. Penner, Phys. Rev. C **71**, 055206 (2005), nucl-th/0412029, [Erratum: Phys.Rev.C 72, 019903 (2005)].
 - [39] A. Müller-Groeling, K. Holinde, and J. Speth, Nucl. Phys. A **513**, 557 (1990).
 - [40] D. Lohse, J. W. Durso, K. Holinde, and J. Speth, Nucl. Phys. A **516**, 513 (1990).
 - [41] B. C. Pearce, K. Holinde, and J. Speth, Nucl. Phys. A **541**, 663 (1992).
 - [42] C. Schütz, K. Holinde, J. Speth, B. C. Pearce, and J. W. Durso, Phys. Rev. C **51**, 1374 (1995), nucl-th/9411022.
 - [43] C. Schütz, J. W. Durso, K. Holinde, and J. Speth, Phys. Rev. C **49**, 2671 (1994).
 - [44] C. Schütz, J. Haidenbauer, J. Speth, and J. W. Durso, Phys. Rev. C **57**, 1464 (1998).
 - [45] O. Krehl, C. Hanhart, S. Krewald, and J. Speth, Phys. Rev. C **62**, 025207 (2000), nucl-th/9911080.
 - [46] A. M. Gasparyan, J. Haidenbauer, C. Hanhart, and J. Speth, Phys. Rev. C **68**, 045207 (2003), nucl-th/0307072.
 - [47] A. Matsuyama, T. Sato, and T. S. H. Lee, Phys. Rept. **439**, 193 (2007), nucl-th/0608051.
 - [48] M. W. Paris, Phys. Rev. C **79**, 025208 (2009), 0802.3383.
 - [49] M. Döring, C. Hanhart, F. Huang, S. Krewald, and U.-G. Meißner, Nucl. Phys. A **829**, 170 (2009), 0903.4337.
 - [50] M. Döring *et al.*, Nucl. Phys. A **851**, 58 (2011), 1009.3781.
 - [51] D. Rönchen *et al.*, Eur. Phys. J. A **49**, 44 (2013), 1211.6998.
 - [52] K. P. Khemchandani, A. Martinez Torres, H. Nagahiro, and A. Hosaka, Phys. Rev. D **88**, 114016 (2013), 1307.8420.
 - [53] D. Rönchen *et al.*, Eur. Phys. J. A **51**, 70 (2015), 1504.01643.
 - [54] Jülich-Bonn-Washington, M. Mai *et al.*, Phys. Rev. C **103**, 065204 (2021), 2104.07312.
 - [55] Jülich-Bonn-Washington, M. Mai *et al.*, Arxiv preprint (2021), 2111.04774.
 - [56] D. Rönchen *et al.*, Eur. Phys. J. A **50**, 101 (2014), 1401.0634, [Erratum: Eur.Phys.J.A 51, 63 (2015)].
 - [57] D. Rönchen, M. Döring, and U.-G. Meißner, Eur. Phys. J. A **54**, 110 (2018), 1801.10458.
 - [58] C.-W. Shen, D. Rönchen, U.-G. Meißner, and B.-S. Zou, Chin. Phys. C **42**, 023106 (2018), 1710.03885.

- [59] Z.-L. Wang, C.-W. Shen, D. Rönchen, U.-G. Meißner, and B.-S. Zou, *Eur. Phys. J. C* **82**, 497 (2022), 2204.12122.
- [60] G. E. Brown and M. Rho, *Phys. Rev. Lett.* **66**, 2720 (1991).
- [61] T. Hatsuda and S. H. Lee, *Phys. Rev. C* **46**, R34 (1992).
- [62] T. D. Cohen, R. J. Furnstahl, and D. K. Griegel, *Phys. Rev. C* **45**, 1881 (1992).
- [63] V. Bernard and U.-G. Meißner, *Nucl. Phys. A* **489**, 647 (1988).
- [64] R. Rapp, J. Wambach, and H. van Hees, *Landolt-Börnstein* **23**, 134 (2010), 0901.3289.
- [65] M. Gell-Mann and F. Zachariasen, *Phys. Rev.* **124**, 953 (1961).
- [66] H. Shen, H. Toki, K. Oyamatsu, and K. Sumiyoshi, *Nucl. Phys. A* **637**, 435 (1998), nucl-th/9805035.
- [67] C. B. Dover, J. Hüfner, and R. H. Lemmer, *Annals Phys.* **66**, 248 (1971).
- [68] Y. Koike and A. Hayashigaki, *Prog. Theor. Phys.* **98**, 631 (1997), nucl-th/9609001.
- [69] F. Klingl, N. Kaiser, and W. Weise, *Nucl. Phys. A* **624**, 527 (1997), hep-ph/9704398.
- [70] F. Klingl, T. Waas, and W. Weise, *Nucl. Phys. A* **650**, 299 (1999), hep-ph/9810312.
- [71] P. Muehlich, V. Shklyar, S. Leupold, U. Mosel, and M. Post, *Nucl. Phys. A* **780**, 187 (2006), nucl-th/0607061.
- [72] I. I. Strakovsky *et al.*, *Phys. Rev. C* **91**, 045207 (2015), 1407.3465.
- [73] V. Metag, M. Nanova, and E. Y. Paryev, *Prog. Part. Nucl. Phys.* **97**, 199 (2017), 1706.09654.
- [74] T. Ishikawa *et al.*, *Phys. Rev. C* **101**, 052201 (2020), 1904.02797.
- [75] Jübo_omegan solution, http://collaborations.fz-juelich.de/ikp/meson-baryon/juelich_amplitudes.html.
- [76] see the attached pdf file SM.OmegaN.pdf, (Supplemental Material) .
- [77] S. S. Schweber, *An Introduction to Relativistic Quantum Field Theory, Etc* (New York; John Weatherhill: Tokyo; printed in Japan, 1964).
- [78] G. Sterman, *An introduction to quantum field theory* (Cambridge university press, 1993).
- [79] J. Wess and B. Zumino, *Phys. Rev.* **163**, 1727 (1967).
- [80] N. M. Kroll, T. D. Lee, and B. Zumino, *Phys. Rev.* **157**, 1376 (1967).
- [81] U.-G. Meißner, *Phys. Rept.* **161**, 213 (1988).
- [82] J. S. Danburg *et al.*, *Phys. Rev. D* **2**, 2564 (1970).
- [83] R. Kraemer *et al.*, *Phys. Rev.* **136**, B496 (1964).
- [84] D. M. Binnie *et al.*, *Phys. Rev. D* **8**, 2789 (1973).
- [85] J. Keyne *et al.*, *Phys. Rev. D* **14**, 28 (1976).
- [86] H. Karami *et al.*, *Nucl. Phys. B* **154**, 503 (1979).
- [87] F. Eisler *et al.*, *Il Nuovo Cimento* (1955-1965) **10**, 468 (1958).
- [88] F. S. Crawford Jr *et al.*, *Physical Review Letters* **3**, 394 (1959).
- [89] C. Baltay *et al.*, *Reviews of Modern Physics* **33**, 374 (1961).
- [90] A. Berthelot *et al.*, *Il Nuovo Cimento* (1955-1965) **21**, 693 (1961).
- [91] L. Bertanza *et al.*, *Phys. Rev. Lett.* **8**, 332 (1962).
- [92] F. S. Crawford, F. Grard, and G. A. Smith, *Phys. Rev.* **128**, 368 (1962).
- [93] L. L. Yoder, C. T. Coffin, D. I. Meyer, and K. M. Terwilliger, *Phys. Rev.* **132**, 1778 (1963).
- [94] J. Keren, *Phys. Rev.* **133**, B457 (1964).
- [95] N. Carayannopoulos, G. Tautfest, and R. Willmann, *Physical Review* **138**, B433 (1965).
- [96] D. Miller, A. Kovacs, R. McIlwain, T. Palfrey, and G. Tautfest, *Physical Review* **140**, B360 (1965).
- [97] P. Daronian *et al.*, *Il Nuovo Cimento A* (1971-1996) **41**, 503 (1966).
- [98] O. Goussu *et al.*, *Nuovo Cim. A* **42**, 606 (1966).
- [99] S. Dagan, Z. M. Ma, J. W. Chapman, L. R. Fortney, and E. C. Fowler, *Phys. Rev.* **161**, 1384 (1967).
- [100] O. I. Dahl *et al.*, *Phys. Rev.* **163**, 1430 (1967), [Erratum: *Phys. Rev.* **183**, 1520 (1969)].
- [101] J. C. Doyle, F. S. Crawford, and J. A. Anderson, *Phys. Rev.* **165**, 1483 (1968).
- [102] T. O. Binford *et al.*, *Phys. Rev.* **183**, 1134 (1969).
- [103] W. Deinet *et al.*, *Nucl. Phys. B* **11**, 495 (1969).
- [104] M. L. Good and R. R. Kofler, *Phys. Rev.* **183**, 1142 (1969).
- [105] O. Van Dyck *et al.*, *Phys. Rev. Lett.* **23**, 50 (1969).
- [106] G. E. Kalmus, G. Borreani, and J. Louie, *Phys. Rev. D* **2**, 1824 (1970).
- [107] Y.-L. Pan, F. L. Forman, W. Ko, V. Hagopian, and W. Selove, *Phys. Rev. D* **2**, 449 (1970).
- [108] W. B. Richards *et al.*, *Phys. Rev. D* **1**, 10 (1970).
- [109] J. J. Jones *et al.*, *Phys. Rev. Lett.* **26**, 860 (1971).
- [110] E. Bellamy *et al.*, *Physics Letters B* **39**, 299 (1972).
- [111] T. M. Knasel *et al.*, *Phys. Rev. D* **11**, 1 (1975).
- [112] A. Berthon, J. Mas, J. L. Narjoux, and P. Ladron De Guevara, *Nucl. Phys. B* **81**, 431 (1974).
- [113] N. C. Debenham *et al.*, *Phys. Rev. D* **12**, 2545 (1975).
- [114] J. Feltesse *et al.*, *Nucl. Phys. B* **93**, 242 (1975).
- [115] M. Winik, S. Toaff, D. Revel, J. Goldberg, and L. Berny, *Nucl. Phys. B* **128**, 66 (1977).
- [116] R. D. Baker *et al.*, *Nucl. Phys. B* **141**, 29 (1978).
- [117] R. D. Baker *et al.*, *Nucl. Phys. B* **156**, 93 (1979).
- [118] R. M. Brown *et al.*, *Nucl. Phys. B* **153**, 89 (1979).
- [119] D. H. Saxon *et al.*, *Nucl. Phys. B* **162**, 522 (1980).
- [120] D. J. Candlin *et al.*, *Nucl. Phys. B* **226**, 1 (1983).
- [121] K. W. Bell *et al.*, *Nucl. Phys. B* **222**, 389 (1983).
- [122] A. Baldini, V. Flamino, W. Moorhead, and D. R. Morrison, *Landolt-börnstein, numerical data and functional relationships in science and technology*, vol. by h. schopper, 1988.
- [123] D. J. Candlin *et al.*, *Nucl. Phys. B* **311**, 613 (1989).
- [124] T. Morrison, *PhD Thesis*, PhD thesis, The George Washington University, 2000.
- [125] R. A. Arndt, W. J. Briscoe, I. I. Strakovsky, R. L. Workman, and M. M. Pavan, *Phys. Rev. C* **69**, 035213 (2004), nucl-th/0311089.
- [126] N. G. Kozlenko *et al.*, *Phys. Atom. Nucl.* **66**, 110 (2003).
- [127] S. Prakhov *et al.*, *Phys. Rev. C* **72**, 015203 (2005).
- [128] D. E. Bayadilov *et al.*, *Eur. Phys. J. A* **35**, 287 (2008).
- [129] Jülich Supercomputing Centre, *Journal of large-scale research facilities* **7** (2021).
- [130] M. I. Haftel and F. Tabakin, *Nucl. Phys. A* **158**, 1 (1970).
- [131] F. James *et al.*, *CERN Program Library Long Writeup D* **506**, 1993 (1994).
- [132] M. Döring, J. Revier, D. Rönchen, and R. L. Workman, *Phys. Rev. C* **93**, 065205 (2016), 1603.07265.
- [133] R. Tibshirani, *J. R. Stat. Soc. B* **58**, 267 (1996).

- [134] P. D. Group *et al.*, Progress of Theoretical and Experimental Physics **2020** (2020), <https://academic.oup.com/ptep/article-pdf/2020/8/083C01/34673722/ptaa104.pdf>, 083C01.
- [135] D. Rönchen, M. Döring, U.-G. Meißner, and C.-W. Shen, Arxiv preprint (2022), 2208.00089.
- [136] A. V. Anisovich *et al.*, Eur. Phys. J. A **48**, 15 (2012), 1112.4937.
- [137] Q. Zhao, Phys. Rev. C **63**, 025203 (2001), nucl-th/0010038.
- [138] E. Friedman and A. Gal, Physics Reports **452**, 89 (2007).
- [139] M. Hoferichter, J. Ruiz de Elvira, B. Kubis, and U.-G. Meißner, Phys. Rept. **625**, 1 (2016), 1510.06039.
- [140] F.-K. Guo *et al.*, Rev. Mod. Phys. **90**, 015004 (2018), 1705.00141, [Erratum: Rev.Mod.Phys. 94, 029901 (2022)].
- [141] Y.-F. Wang, D.-L. Yao, and H.-Q. Zheng, Eur. Phys. J. C **78**, 543 (2018), 1712.09257.
- [142] Y.-F. Wang, D.-L. Yao, and H.-Q. Zheng, Front. Phys. (Beijing) **14**, 24501 (2019), 1810.07958.
- [143] Y.-F. Wang, D.-L. Yao, and H.-Q. Zheng, Chin. Phys. C **43**, 064110 (2019), 1811.09748.
- [144] Y. Ma, W.-Q. Niu, Y.-F. Wang, and H.-Q. Zheng, Commun. Theor. Phys. **72**, 105203 (2020), 2002.02351.
- [145] Q.-Z. Li, Y. Ma, W.-Q. Niu, Y.-F. Wang, and H.-Q. Zheng, Chin. Phys. C **46**, 023104 (2022), 2102.00977.
- [146] C. Chen, W.-Q. Niu, and H.-Q. Zheng, Arxiv preprint (2022), 2203.03747.
- [147] X.-H. Cao, Q.-Z. Li, and H.-Q. Zheng, Arxiv preprint (2022), 2207.09743.